RESEARCH ARTICLE SUMMARY

PSYCHENCODE2

Systems biology dissection of PTSD and MDD across brain regions, cell types, and blood

Nikolaos P. Daskalakis* *et al.*,

INTRODUCTION: Stress-related disorders arise from the interplay between genetic susceptibility and stress exposure, occurring throughout the lifespan. Progressively, these interactions lead to epigenetic modifications in the human genome, shaping the expression of genes and proteins. Prior postmortem brain studies have attempted to elucidate the molecular pathology of posttraumatic stress disorder (PTSD) and major depressive disorder (MDD) compared with neurotypical controls (NCs) in a single-omic manner, revealing genomic overlap, sex differences, and immune and interneuron signaling involvement. However, without integrative systems approaches, progress in understanding the molecular underpinnings of these prevalent and debilitating disorders is hindered.

RATIONALE: To tackle this roadblock, we have created a brain multiregion, multiomic database of individuals with PTSD and MDD and NCs (77 per group, n = 231) to describe molecular alterations across three brain regions: the central nucleus of the amygdala (CeA), medial prefrontal cortex (mPFC), and hippocampal dentate gyrus (DG) at the transcriptomic, methylomic, and proteomic levels. By using this multiomic strategy that merges information across biological layers and organizational strata and complementing it with single-nucleus RNA sequencing (snRNA-seq), genetics, and blood plasma proteomics analyses, we sought to reveal an integrated-systems perspective of PTSD and MDD.

RESULTS: We found molecular differences primarily in the mPFC, with differentially expressed genes (DEGs) and exons carrying the most disease signals. However, altered methylation was seen mainly in the DG in PTSD subjects, in contrast to the CeA in MDD subjects. Replication analysis substantiated these findings with multiomic data from two cohorts (n = 114). Moreover, we found a moderate overlap between the disorders, with childhood trauma and suicide being primary drivers of molecular variations in both disorders, and sex specificity being more notable in MDD. Pathway analyses linked disease-associated molecular signatures to immune mechanisms, metabolism, mitochondria function, neuronal or synaptic regulation, and stress hormone signaling with low concordance across omics. Top upstream regulators and transcription factors included IL1B, GR, STAT3, and TNF. Multiomic factor and gene network analyses provided an underlying genomic structure of the disorders, suggesting latent factors and modules related to aging, inflammation, vascular processes, and stress.

To complement the multiomics analyses, our snRNA-seq analyses in the dorsolateral PFC (n = 118) revealed DEGs, dysregulated pathways, and upstream regulators in neuronal and non-neuronal cell-types, including stress-related gene signals. Examining the intersection of brain multiomics with blood proteins (in >50,000 UK Biobank participants) revealed significant correlation, overlap, and directional similarity between brain-to-blood markers. Fine-mapping of PTSD and MDD genome-wide association studies' (GWASs') results showed a limited overlap between risk and disease processes at the gene and pathway levels.

Ultimately, prioritized genes with multiregion, multiomic, or multitrait disease associations were members of pathways or networks, showed cell-type specificity, had blood biomarker potential, or were involved in genetic risk for PTSD and MDD.

CONCLUSION: Our findings unveil shared and distinct brain multiomic molecular dysregulations in PTSD and MDD, elucidate the involvement of specific cell types, pave the way for the development of blood-based biomarkers, and distinguish risk from disease processes. These insights not only implicate established stress-related pathways but also reveal potential therapeutic avenues. ■

The list of author affiliations is available in the full article online.
*Corresponding authors: Nikolaos P. Daskalakis (ndaskalakis@mclean.harvard.edu); Kerry J. Ressler (kressler@mclean.harvard.edu)
Cite this article as N. Daskalakis *et al.*, *Science* **384**, eadh3707 (2024). DOI: 10.1126/science.adh3707

READ THE FULL ARTICLE AT
https://doi.org/10.1126/science.adh3707

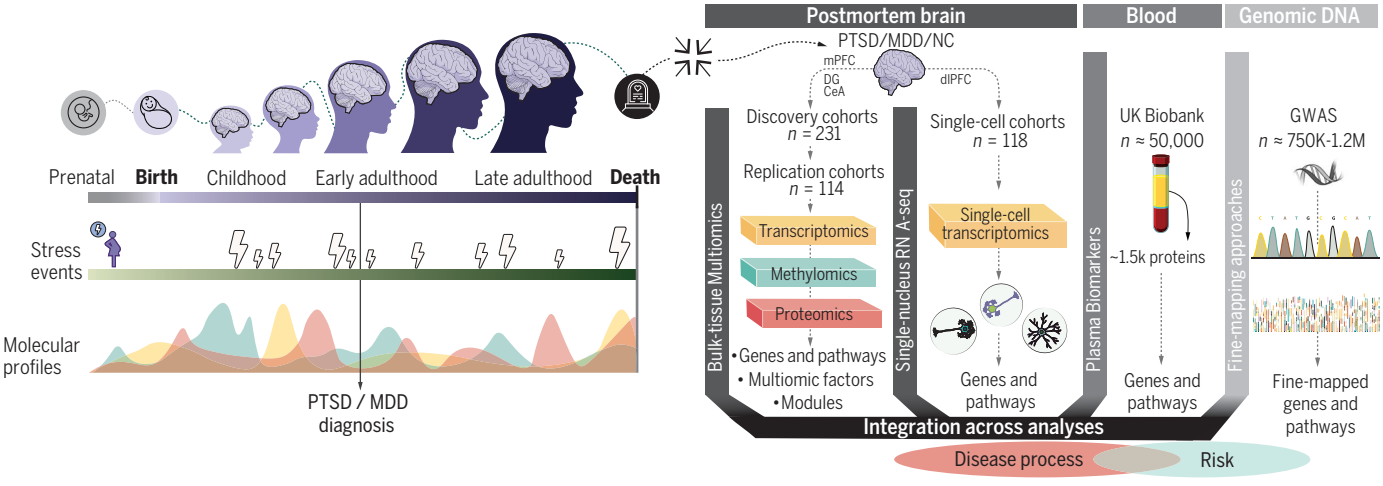

Systems biology dissection of PTSD and MDD. The interplay between genetic susceptibility and stress exposure, occurring both early and later in life, contributes to the pathogenesis of stress-related disorders and their progression after diagnosis until death. Our integrative systems approach combines multiregion, multiomic analyses with single-nucleus transcriptomics, blood plasma proteomics, and GWAS-based fine-mapping to provide deeper insights into molecular mechanisms associated with risk and those involved in the disease process.

RESEARCH ARTICLE

PSYCHENCODE2

Systems biology dissection of PTSD and MDD across brain regions, cell types, and blood

Nikolaos P. Daskalakis[1,2,3]*, Artemis Iatrou[1,2,3]†, Chris Chatzinakos[1,3,4,5]†, Aarti Jajoo[1,2,3]†, Clara Snijders[1,2,3]†, Dennis Wylie[6]‡, Christopher P. DiPietro[1,3]‡, Ioulia Tsatsani[1,2,3,7]‡, Chia-Yen Chen[8]§, Cameron D. Pernia[1,2,3]§, Marina Soliva-Estruch[1,2,3,7]§, Dhivya Arasappan[6]¶, Rahul A. Bharadwaj[9]¶, Leonardo Collado-Torres[9]¶, Stefan Wuchty[10,11]¶, Victor E. Alvarez[12,13,14]#, Eric B. Dammer[15]#, Amy Deep-Soboslay[9]#, Duc M. Duong[15]#, Nick Eagles[9]#, Bertrand R. Huber[12,14]#, Louise Huuki[9]#, Vincent L. Holstein[1,2,3]#, Mark W. Logue[16,17,18,19]#, Justina F. Lugenbühl[1,2,3,7]#, Adam X. Maihofer[20,21,22]#, Mark W. Miller[16,17]#, Caroline M. Nievergelt[20,21,22]#, Geo Pertea[9]#, Deanna Ross[23]#, Mohammad S. E. Sendi[1,2,3]#, Benjamin B. Sun[8]#, Ran Tao[9]#, James Tooke[9]#, Erika J. Wolf[16,17]#, Zane Zeier[24]#, PTSD Working Group of Psychiatric Genomics Consortium**, Sabina Berretta[1,2,3]††, Frances A. Champagne[23]††, Thomas Hyde[9,25,26]††, Nicholas T. Seyfried[15]††, Joo Heon Shin[9,26]††, Daniel R. Weinberger[9,25,26,27,28]††, Charles B. Nemeroff[23,29]‡‡, Joel E. Kleinman[9,25]‡‡, Kerry J. Ressler[1,2]*‡‡

The molecular pathology of stress-related disorders remains elusive. Our brain multiregion, multiomic study of posttraumatic stress disorder (PTSD) and major depressive disorder (MDD) included the central nucleus of the amygdala, hippocampal dentate gyrus, and medial prefrontal cortex (mPFC). Genes and exons within the mPFC carried most disease signals replicated across two independent cohorts. Pathways pointed to immune function, neuronal and synaptic regulation, and stress hormones. Multiomic factor and gene network analyses provided the underlying genomic structure. Single nucleus RNA sequencing in dorsolateral PFC revealed dysregulated (stress-related) signals in neuronal and non-neuronal cell types. Analyses of brain-blood intersections in >50,000 UK Biobank participants were conducted along with fine-mapping of the results of PTSD and MDD genome-wide association studies to distinguish risk from disease processes. Our data suggest shared and distinct molecular pathology in both disorders and propose potential therapeutic targets and biomarkers.

The development of stress-related disorders, such as posttraumatic stress disorder (PTSD) and major depressive disorder (MDD), involves complex interactions between genetic susceptibility and exposure to traumatic stress. Over the last two decades, substantial efforts have focused on identifying the underlying risk factors and molecular mechanisms as well as tackling the high rates of comorbidity and disorder heterogeneity associated with PTSD and MDD.

Genome-wide association studies (GWAS) revealed the heritability, polygenic architecture, and genetic overlap of PTSD and MDD (*1*–*6*). Previous work profiling molecular alterations of stress-related mental disorders in blood (*7*–*13*) has implicated the innate immune response and regulation by stress hormones such as glucocorticoids (GC), but conclusions have been limited owing to lack of direct access to the brain and its cell types. The availability of new, large, well-characterized postmortem brain collections of PTSD and MDD subjects and neurotypical controls (NCs) (*14*) enabled the investigation of brain-based molecular alterations. Genome-wide transcriptomic and methylomic studies of prefrontal cortex (PFC) subregions (*15*–*19*) and amygdala (AMY) nuclei (*17*) in PTSD and MDD revealed a moderate genomic overlap and sex differences, confirmed immune dysregulations, and implicated both interneuron- and glia-based signaling. These studies converged with parallel functional analyses of GWAS loci (*20*, *21*). Targeted transcriptomic and proteomic postmortem analyses also focused on disease associations with expression of immune- and stress-related genes (*22*). Single-nucleus RNA sequencing (snRNA-seq) suggested some neuronal and non-neuronal cell types related to risk loci, stress pathways, and/or sex differences (*23*–*25*).

Despite recent progress, reductionist single-omic approaches, although valuable, likely miss a comprehensive picture. Multiomic approaches combining data from genetics, transcriptomics, epigenomics, and proteomics, among others, may unveil an integrative systems view of stress-related diseases (*26*, *27*). In this work, we provide a systematic characterization of a large multiregion, multiomic dataset of PTSD and MDD generated by the PTSD Brainomics Project of the PsychENCODE Consortium (PEC) Phase 2 (Fig. 1). The dataset consists of three brain regions [medial PFC (mPFC), dentate gyrus (DG) of the hippocampus (HIP), and central nucleus of AMY (CeA)] from 231 subjects with PTSD and/or MDD versus NCs split over two cohorts. We interrogated disease-specific molecular changes at four transcriptomic levels [~22,000 genes, ~335,000 exons, ~140,000 exon-exon junctions (jxs), and ~198,000 transcripts (txs)], one methylated DNA (mDNA) level [~740,000 cytosine-phosphate-guanine

[1]McLean Hospital, Belmont, MA 02478, USA. [2]Department of Psychiatry, Harvard Medical School, Boston, MA 02115, USA. [3]Stanley Center for Psychiatric Research, Broad Institute of MIT and Harvard, Cambridge, MA 02142, USA. [4]Department of Psychiatry and Behavioral Sciences, SUNY Downstate Health Sciences University, Brooklyn, NY 11203, USA. [5]VA New York Harbor Healthcare System, Brooklyn, NY 11209, USA. [6]Center for Biomedical Research Support, The University of Texas at Austin, Austin, TX 78712, USA. [7]Department of Psychiatry and Neuropsychology, School for Mental Health and Neuroscience (MHeNs), Maastricht University, Maastricht, 6229 ER, Netherlands. [8]Biogen Inc., Cambridge, MA 02142, USA. [9]Lieber Institute for Brain Development, Johns Hopkins Medical Campus, Baltimore, MD 21205, USA. [10]Departments of Computer Science, University of Miami, Miami, FL 33146, USA. [11]Department of Biology, University of Miami, Miami, FL 33146, USA. [12]Department of Neurology, Boston University, Chobanian & Avedisian School of Medicine, Boston, MA 02118, USA. [13]VA Bedford Healthcare System, Bedford, MA 01730, USA. [14]National Posttraumatic Stress Disorder Brain Bank, VA Boston Healthcare System, Boston, MA 02130, USA. [15]Department of Biochemistry, Center for Neurodegenerative Disease, Emory School of Medicine, Atlanta GA 30329, USA. [16]National Center for PTSD, VA Boston Healthcare System, Boston, MA 02130, USA. [17]Department of Psychiatry, Boston University Chobanian & Avedisian School of Medicine, Boston, MA 02118, USA. [18]Department of Biomedical Genetics, Boston University Chobanian & Avedisian School of Medicine, Boston, MA 02118, USA. [19]Department of Biostatistics, Boston University School of Public Health, Boston, MA 02118, USA. [20]Department of Psychiatry, University of California San Diego, La Jolla, CA 92093, USA. [21]Center for Excellence in Stress and Mental Health, Veterans Affairs San Diego Healthcare System, San Diego, CA 92161, USA. [22]Research Service, Veterans Affairs San Diego Healthcare System, San Diego, CA 92161, USA. [23]Department of Psychology, University of Texas at Austin, Austin, TX 78712, USA. [24]Department of Psychiatry & Behavioral Sciences, Center for Therapeutic Innovation, University of Miami Miller School of Medicine, Miami, FL 33136, USA. [25]Department of Psychiatry and Behavioral Sciences, Johns Hopkins University School of Medicine; Baltimore, MD, 21205, USA. [26]Department of Neurology, Johns Hopkins University School of Medicine, Baltimore, MD 21205, USA. [27]Department of Neuroscience, Johns Hopkins University School of Medicine, Baltimore, MD 21205, USA. [28]Department of Genetic Medicine, Johns Hopkins University School of Medicine, Baltimore, MD 21205, USA. [29]Department of Psychiatry and Behavioral Sciences, University of Texas at Austin, Austin, TX 78712, USA.
***Corresponding author. Email: ndaskalakis@mclean.harvard.edu (N.P.D.); kressler@mclean.harvard.edu (K.J.R.)**
†These authors contributed equally to this work.
‡These authors contributed equally to this work.
§These authors contributed equally to this work.
¶These authors contributed equally to this work.
#These authors contributed equally to this work.
**PTSD Working Group of Psychiatric Genomics Consortium collaborators are listed in the supplementary materials.
††These authors contributed equally to this work.
‡‡These authors contributed equally to this work.

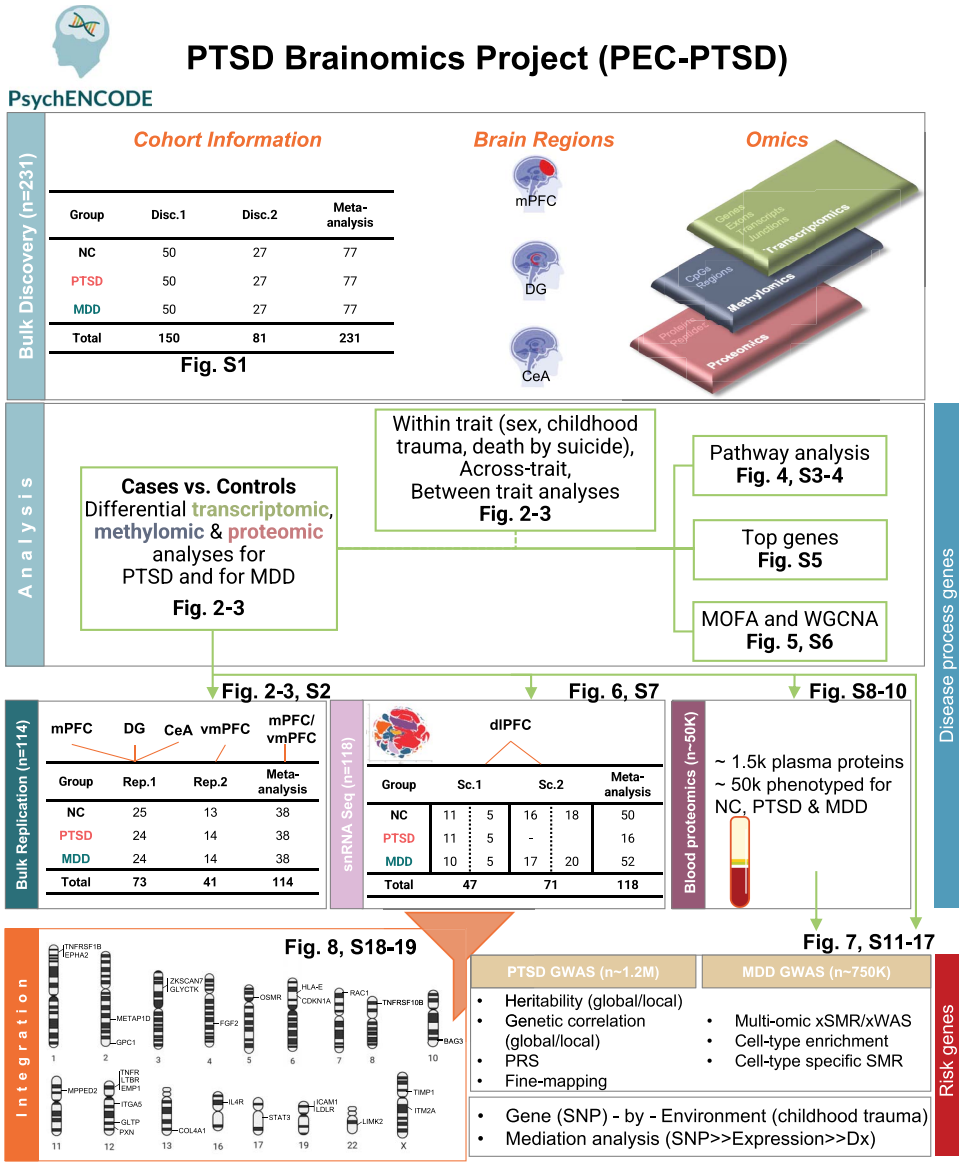

Fig. 1. Overall study design. We generated a large multiregion, multiomic postmortem brain database of PTSD (n = 77) and MDD (n = 77) compared with NC (n = 77) over two discovery cohorts (Disc.1 and Disc.2). Three brain regions (mPFC, DG, and CeA) were assessed for bulk RNA expression (of genes, exons, exon-exon junctions, and transcripts), DNA methylation (CpGs and regions), and protein expression (proteins and peptides). Primary analyses included differential transcriptomic, methylomic, and proteomic disease-specific interrogation, followed by pathway, multiomic factor, and gene coexpression network analyses and identification of top genes. Subanalyses were performed within traits (i.e., biological sex, childhood trauma, and suicide completion), across traits (PTSD-or-MDD versus NC) and between traits (PTSD versus MDD) to assess contributing factors, disease specificity, and overlap. For replication, we (i) generated a new multiregion, multiomic dataset of samples from 73 subjects (Rep.1), reanalyzed data from prior studies (Rep.2) consisting of 41 additional samples from ventromedial PFC (vmPFC), and (ii) conducted meta-analysis of these two independent cohorts ($n_{meta\text{-}analysis}$ = 114). In parallel, we (i) acquired two snRNA-seq datasets (Sc.1, n = 47; Sc.2, n = 71) from dlPFC in two batches each to explore disease-associated cell type–specific transcriptomic signatures by conducting meta-analysis across batches ($n_{meta\text{-}analysis}$ = 118), (ii) assessed the blood plasma protein–based biomarker potential in >50,000 subjects of the UKBB, and (iii) fine-mapped the PTSD and MDD risk loci using GWAS datasets and investigated the overlap of GWAS-based risk genes and pathways with disease process genes. The extensive generated data enabled us to identify genes significantly involved in both disorders. Dx, diagnosis.

sites (CpGs)] and two proteomic levels [~6200 proteins and ~60,000 peptides]. Replication was tested in equivalent datasets from up to 114 additional subjects. Analyses were complemented by a rigorous exploration of downstream pathways, multiomic latent factors, and gene networks. In parallel, we tackled cell-type specificity by conducting snRNA-seq analysis of 118 dorsolateral PFC (dlPFC) samples (*23*–*25*), and evaluated blood-based protein biomarkers in >50,000 UK Biobank (UKBB) participants. Lastly, PTSD and MDD risk was captured by the largest currently available GWAS datasets (*5*, *6*), allowing investigation of the overlap of GWAS-based risk genes with our postmortem brain-based disease process genes [defined in (*28*)]. Our results suggested that multiregion, multiomic mechanisms underlie shared and distinct brain pathology in PTSD and MDD and that they overlap with cell type–specific, blood-based and genetically mediated mechanisms.

Multiregion, multiomic signatures in PTSD and MDD

Discovery cohorts 1 ["Disc.1," 50/group (150 total) (table S1A-1)] and 2 ["Disc.2," 27/group (81 total) (table S1A-2)] were initially analyzed separately. No significant differences were found between disease groups and NCs in cell-type proportions, as estimated from RNA genes or CpGs (tables S1B-1 and S1B-2). We then meta-analyzed the results from both cohorts and revealed multiregion, multiomic alterations for both disorders (PTSD, Fig. 2 and table S2A, 1 to 21; MDD, Fig. 3 and table S2B, 1 to 21). Most differential gene expression (DGE) signals passing the 5% false discovery rate (FDR) level were found in mPFC for both PTSD (Fig. 2A) and MDD (Fig. 3A), with differentially expressed genes (DEGs) and exons leading, followed by jxs in PTSD, and txs in MDD. In the other brain regions, genes and exons in MDD showed a substantial number of FDR-significant signals (FDR-adjusted $P < 0.05$). We found many differentially methylated positions (DMPs) in the DG in PTSD (Fig. 2B) and less in MDD (Fig. 3B). Similarly, differentially methylated regions (DMRs) were mainly observed in the DG in PTSD (95) (Fig. 2B and table S2C) and the CeA (17) and DG (13) in MDD (Fig. 3B and table S2C). PTSD had slightly less differentially expressed proteins (DEPs) and peptides (Fig. 2C) compared with MDD (Fig. 3C). These findings were confirmed by counting FDR-significant distinct genes in both PTSD (Fig. 2D) and MDD (Fig. 3D).

We ran mega-analyses and sensitivity analyses focused on multiancestry composition (fig. S1) and RNA quality to ensure the robustness of our results. Results were strongly correlated

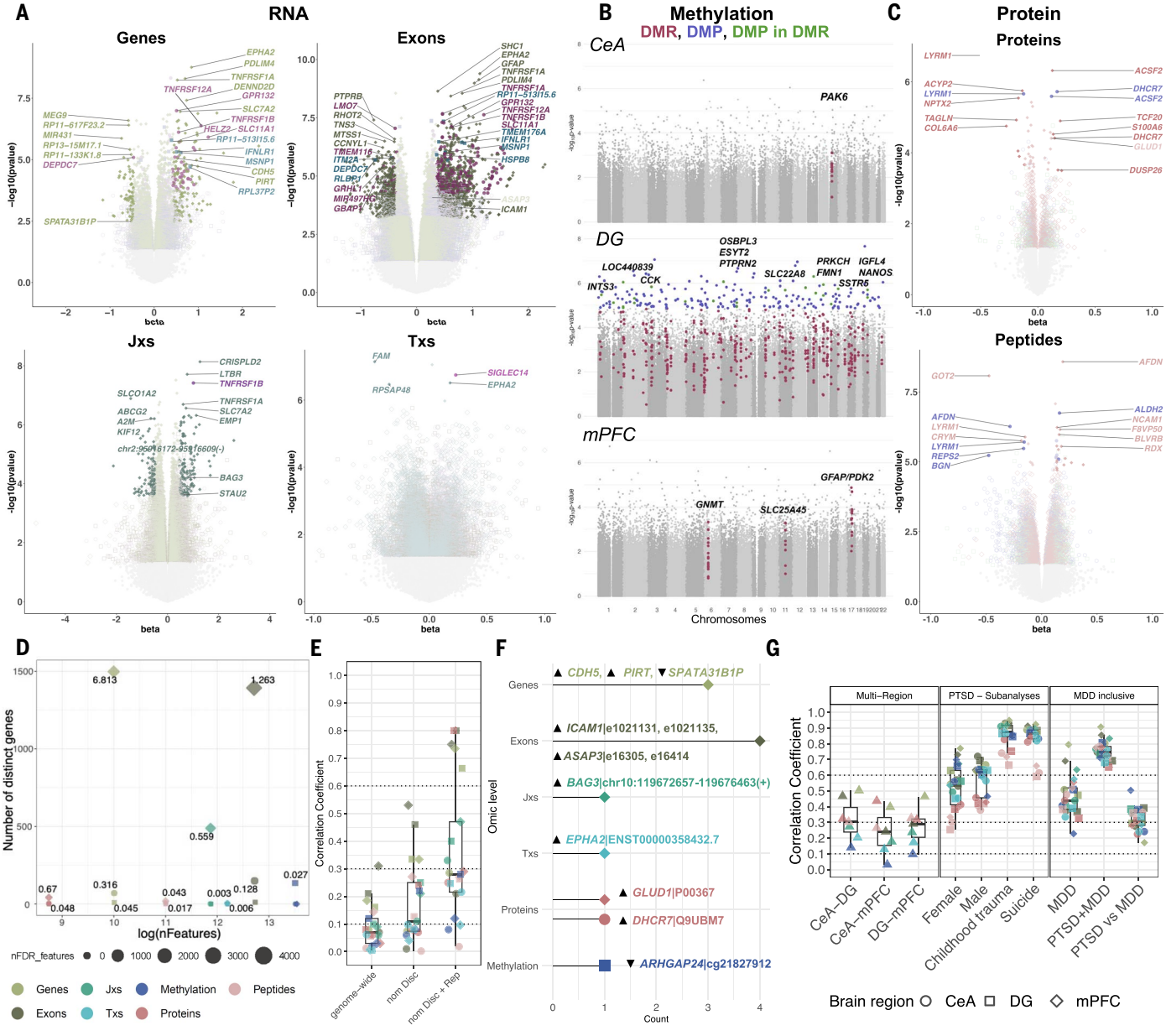

Fig. 2. Transcriptomic, methylomic, and proteomic analyses of PTSD in three brain regions. (**A** to **C**) Plots of the meta-analysis of 231 subjects in mPFC, DG, and CeA. [(A) and (C)] Volcano plots of differentially regulated transcriptomic (A) and proteomic features (C). Colored dots denote nominally significant genes ($P < 0.05$), with the darker ones passing FDR-adjusted $P < 0.05$. Five features with the lowest P in each direction and the replicated ones [see details in (F)] are named. (B) Manhattan plots of the CpGs interrogated for differential methylation (x axis, genomic location; y axis, $-\log_{10}P$). DMPs passing FDR-adjusted $P < 0.05$ are denoted in purple. CpGs that belong to a DMR (>2 CpGs, Šidák $P < 0.05$) are red, and within those, the CpGs with FDR-adjusted $P < 0.05$ are green. (**D**) Scatterplot denoting the number of distinct genes corresponding to FDR-significant features (size coded) per feature type per brain region. The percentage of FDR-adjusted features over the N of features is labeled next to the respective point. (**E**) Boxplot of ρ corresponding to correlations of effect sizes ($\log_2$FC or beta) in discovery meta-analysis ("Disc") and Rep.1 cohort analysis ("Rep") across brain regions. Three significance thresholds were used: "genome-wide" (no threshold), considering all features; "nom Disc," considering only nominally significant ($P < 0.05$) features in Disc; and "nom Disc +Rep," considering overlapping nominally significant features in Disc and Rep. (**F**) Lollipop plots of the number of replicated features per omic type with their respective gene and protein annotations and direction of effect (upward black arrowheads, increased; downward black arrowheads, decreased). (**G**) (Left) Multiregion boxplots depicting the range of ρ corresponding to correlations of effect sizes between PTSD differential analyses of each brain region for each feature. (Middle) Boxplots depicting the range of ρ between PTSD differential analyses results with results from subanalyses, including sex specificity, childhood trauma, and suicide completion, across brain regions. (Right) Boxplots of ρ between PTSD differential analyses results with results from MDD primary analysis and PTSD-or-MDD and PTSD versus MDD subanalyses. In (D) to (G), colors denote different omic features and shape different brain regions. In (E) and (G), horizontal dotted lines denote minimal ($\rho < 0.1$), moderate ($0.3 < \rho < 0.6$), and high ($\rho > 0.6$) correlation.

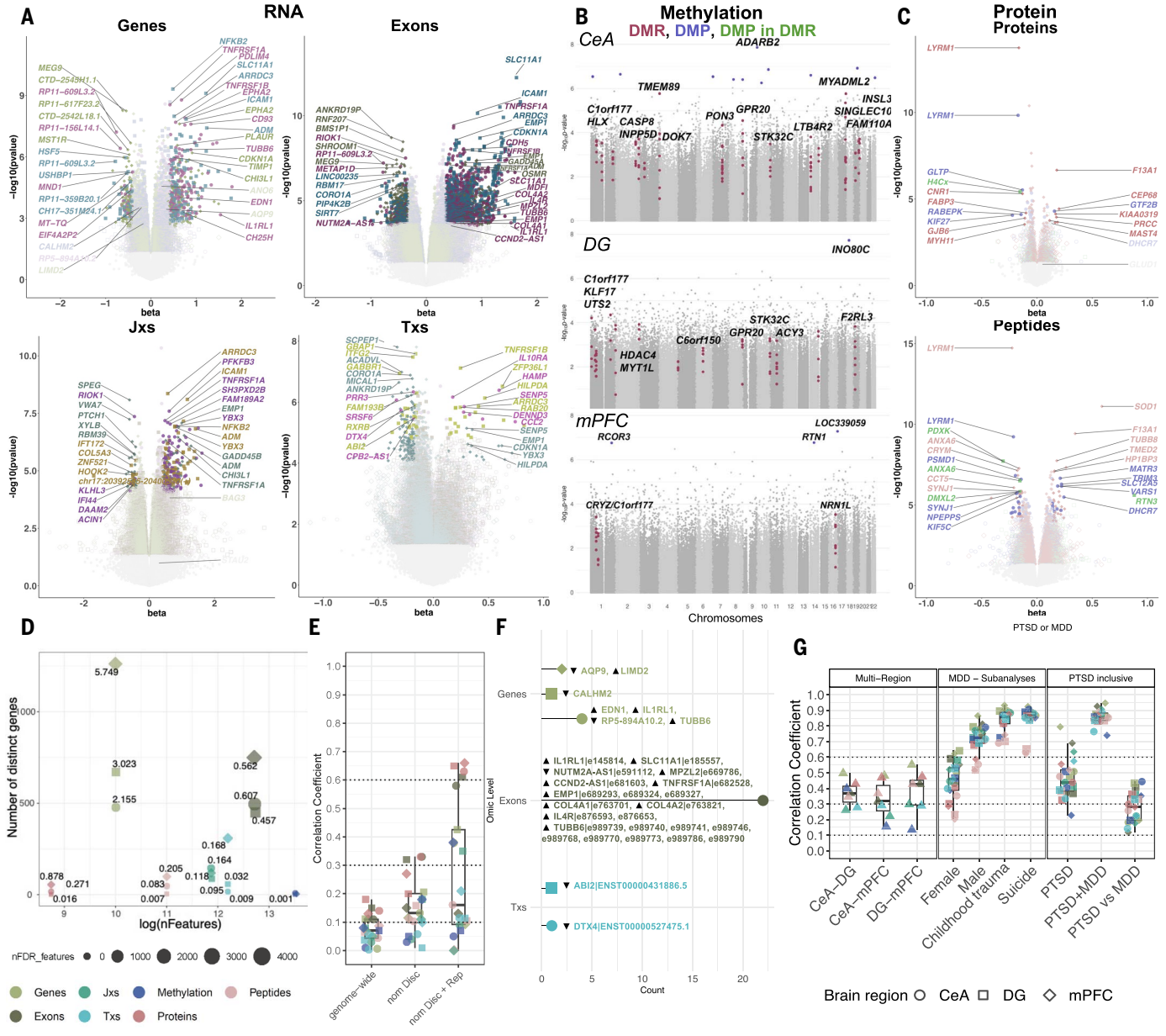

Fig. 3. Transcriptomic, methylomic, and proteomic analyses of MDD in three brain regions. See legend of Fig. 2 for detailed description. (**A** and **C**) Volcano plots of differentially regulated transcriptomic (A) and differentially expressed proteomic features (C). (**B**) Manhattan plots of CpGs with genomic loci on the *x* axis and $-\log_{10}P$ on the *y* axis. Red, Šidák *P*–significant DMRs; purple, FDR-significant DMPs; green, DMPs within DMRs. (**D**) Scatterplot denoting the number of distinct genes corresponding to FDR-significant features (size coded) per feature type per brain region, with the respective percentage labeled. (**E**) Boxplot of correlation coefficient ρ of effect sizes ($\log_2$FC or beta) in discovery meta-analysis ("Disc") and Rep.1 cohort analysis ("Rep") across brain regions and three significance thresholds. (**F**) Lollipop plots of the number of replicated features per omic type with their respective gene and protein annotations and direction of effect (upward arrowheads, increased; downward arrowheads, decreased). (**G**) (Left) Boxplots of correlation coefficient ρ of effect sizes between MDD analyses of each brain region for each feature. (Middle) Boxplots depicting the range of ρ between MDD primary analyses with subanalyses across brain regions. (Right) Boxplots of ρ between MDD differential analyses results with results from PTSD primary analysis and PTSD-or-MDD and PTSD versus MDD subanalyses. In (D) to (G), colors denote different omic features and shape different brain regions. In (E) and (G), horizontal dotted lines denote minimal ($\rho < 0.1$), moderate ($0.3 < \rho < 0.6$), and high ($\rho > 0.6$) correlation.

with those from the discovery meta-analysis [fig. S2A; for details, see (*28*)].

Replication analyses

We analyzed data from two replication cohorts ["Rep.1," 24/group (table S3A, 1 and 2); "Rep.2:" 14/group (table S3B, 1 and 2)] with details described in (*28*). The majority of the correlations of discovery meta-analysis with Rep.1 results were moderate to high (Spearman's ρ = 0.3 to 0.6), indicating concordant associations (Figs. 2E and 3E and fig. S2B). The correlation drivers were feature type (F test, $P = 7.36 \times 10^{-8}$; RNA > protein > mDNA), brain region (F test, $P = 7.91 \times 10^{-7}$; DG > mPFC > CeA), and statistical threshold (F test, $P = 5.30 \times 10^{-6}$). FDR-significant features in discovery meta-analyses showed beyond-chance rate of concordant direction and nominal significance ($P < 0.05$) in Rep.1 results (PTSD, table S3C, 1 to 21; MDD, table S3C, -22 to -42; enrichment tests, table S3D),

which included 43 replicated features (11 PTSD and 32 MDD) with FDR-adjusted $P < 0.05$ in Rep.1 mapped to 28 distinct genes (table S3, E and F). For Rep.2 (fig. S2B), we confirmed stronger correlations at the gene level compared with methylation. Meta-analysis of Rep.1 and Rep.2 revealed concordant replicated DEGs to discovery cohorts in PTSD (binomial $P = 2.42 \times 10^{-184}$) and MDD (binomial $P = 4.33 \times 10^{-91}$), adding three replicated RNA genes for each trait (table S3, E and F).

Out of 49 replicated features, 43 had the same direction as the discovery meta-analysis (Figs. 2F and 3F). Out of 14 PTSD replicated features (10 genes), 12 were found in the mPFC, and 29 of 35 MDD replicated features (16 genes) were found in the CeA. PTSD replicated genes were more related to brain cell types (notable examples include up-regulation of *EPHA2* and *PIRT*, *ARHGAP24* hypermethylation, and increased GLUD1 protein expression; table S3E) compared with replicated MDD genes reflecting elevated cytokine signaling (table S3F).

Between-region correlations

Within the primary PTSD and MDD analyses, we found weak to moderate between-region correlations of effect sizes (ρ range 0.3 to 0.6) across omics. Moderate correlations were found at the gene, protein, MDD peptide and exon across-region pairs, PTSD exons at the CeA-DG pair, PTSD peptides at the DG-mPFC pair, and MDD CpGs at the CeA-DG pair (Figs. 2G and 3G, left).

Correlations of primary analyses with subanalyses

We performed subanalyses distinguishing (i) biological sex and (ii) cases with childhood trauma or death by suicide. We reported moderate to strong ($\rho > 0.6$) correlations of primary analyses. Female-specific analyses for both disorders demonstrated moderate correlations with their respective primary analyses. By contrast, male-specific analyses in PTSD showed moderate correlations with the primary analyses of PTSD, whereas those in MDD exhibited strong correlations with the primary analyses of MDD. Additionally, analyses focusing on childhood trauma and suicide within both disorders displayed strong correlations with their respective primary analyses. Proteins and peptides had the lowest correlations among all these analyses (Fig. 2G and 3G, middle). Such observations confirm the role of these factors in the overall disease effects and suggest that distinct multiomic features may underlie both PTSD and MDD disease processes in females.

Correlations with other trait, across-trait, and between-trait analyses

Most cases with primary PTSD diagnosis had secondary depression (table S1A, 1 and 2), whereas none of the MDD cases had a secondary PTSD diagnosis. The correlation between PTSD and MDD primary analyses was moderate except for high correlations at the gene, exon, and jx level of mPFC, as well as low correlations of CpGs in the mPFC, which emphasized the importance of epigenetic data in distinguishing the two disorders (Fig. 2G and 3G, right). We also conducted additional analyses comparing (i) all cases ("PTSD-or-MDD"/combined) to NCs and (ii) PTSD cases to MDD cases. The correlation of the primary analysis with combined analysis was high, with mPFC data (especially genes and exons) showing the highest correlations (Fig. 2G and 3G, right). The correlation of PTSD primary analysis with the PTSD versus MDD analysis was moderate, whereas the correlation of MDD analysis with the absolute (PTSD versus MDD) analysis was weak (Fig. 2G and 3G, right).

Functional annotation of multiregion, multiomic signatures

To identify disease-associated pathways, we performed gene set enrichment analysis (GSEA) based on gene ontology (GO) across omics (table S4A, 1 to 18). Ranking pathways on the basis of significance per modality revealed clustering of omic layers in both traits (Fig. 4A). Immune-related biological processes were up-regulated at the transcriptome level, whereas adaptive and innate immunity subsets were down-regulated at the proteome level. Methylomic signatures mostly related to nervous system, axon, and synapse development. Biological processes related to RNA metabolism and transcription were up-regulated at the proteome level. Regarding cellular components, ribosomes were up-regulated at the transcriptome level and down-regulated at the proteome level. Down-regulated proteomic signatures were associated with presynaptic cellular components, whereas methylomic signatures of MDD related to neuron-to-neuron synaptic functions.

Within brain regions, pathways showed absent to weak correlations between omics (Fig. 4B). The highest correlations ($\rho > 0.25$) were observed between RNA-protein and RNA-methylation in the DG of PTSD and RNA-methylation in the CeA of MDD. Between-region correlations ranged from weak to high (Fig. 4C) with transcriptomic pathways showing higher correlations ($\rho > 0.60$) compared with that of proteomic ($0.2 < \rho < 0.40$) and methylomic ($0.05 < \rho < 0.45$) pathways. RNA pathways had the highest correlations between traits (Fig. 4D). These analyses thus suggest that different omic signals are involved in distinct pathways and that, within omics, transcriptomic-based pathways tend to be most conserved between regions (Fig. 4C) and traits (Fig. 4D).

We repeated pathway analyses using Rep.1 results to assess replication of our discovery pathways. Discovery pathways correlated with Rep.1 pathways considerably at the transcriptomic level followed by the proteomic and methylomic levels (fig. S3). PTSD pathways replicated more than MDD pathways (573 versus 91; table S4A-19), most of which were from mPFC RNA (389), DG mDNA (85), and CeA RNA (83). For MDD, replicated pathways were from CeA and DG RNA (35 and 23, respectively) and DG and mPFC mDNA (14 and 12, respectively).

Canonical pathway (CP) enrichment in PTSD and MDD DEGs and DEPs across regions (table S4B) revealed shared DEG-driven up-regulation of immune pathways related to extracellular matrix (ECM) organization including activin and inhibin, hepatic fibrosis, cytokine storm signaling, and STAT3 signaling pathways, mostly in the mPFC for PTSD (Fig. 4E) and DG for MDD (Fig. 4F). MDD DEGs in CeA and DG pointed to the down-regulation of liver X receptor (LXR) and retinoid X receptor (RXR) regulatory pathways, and PTSD DEPs in DG implicated the complement system.

To identify regulatory changes in PTSD and MDD, we identified upstream regulators (URs) of the RNA signals (table S4C). IL1B, TNF, IFNG, CREB1, TGFB1, and OSM were the most prominently activated URs in both disorders, whereas immunoglobin G, SCD, mir-155, PPARGC1A, DICER1, and glutamine were the most deactivated URs (Fig. 4G, table S4C). We then identified enriched transcription factor (TF) binding on the genes of our disease-associated features (table S4D) with lowest enrichment Fisher's exact test (FET) *P* seen in *ESR1*, *ELK3*, *NR3C1* [glucocorticoid receptor (GR)], *RELB*, and *RUNX1* (Fig. 4H).

Spatial registration of transcriptomic and proteomic signatures

We spatially registered the DEGs and DEPs within cortical layers 1 to 6 (L1 to L6) and white matter. We found meningeal and L1 enrichment of DEGs in PTSD and MDD (fig. S4A) but deeper L4 to L5 enrichment of DEPs in MDD (fig. S4B). Leptomeninges and L1 contain mostly non-neuronal cells, whereas deeper cortical layers contain mostly neuronal cells (*29*), highlighting the importance of deciphering cell-type specificity.

Prioritizing top genes and pathways from multiregion, multiomic signatures

To identify key genes associated with stress-related disorders, we integrated FDR-significant signals across omic features, brain regions, and traits amounting to 4469 genes (2677 PTSD, 2970 MDD, and 1178 shared; fig. S5 and table S5A). Demanding a signal in at least half the features within each omic modality for a given trait, we found 1690 genes (table S5B); 1016 were related to PTSD, 1043 to MDD, and 369 to both. These genes were categorized on the basis of the omic layer of their disease-associated signal (1355 RNA, 146 mDNA, and 223 protein), with 34 genes having signal in two omic layers. Notably, these 1690 genes were also

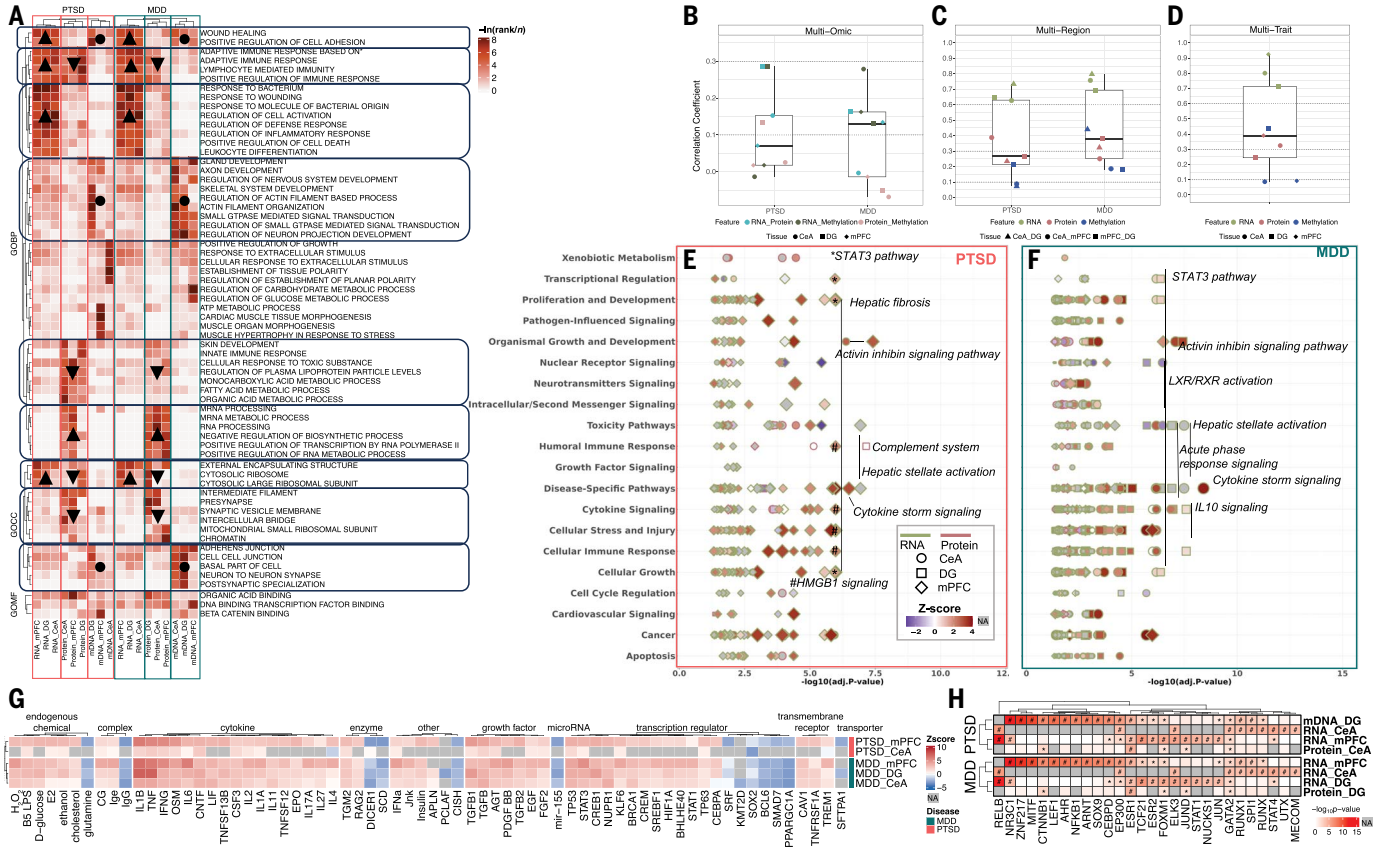

Fig. 4. Transcriptomic-, proteomic-, and methylomic-based gene set enrichment analysis across brain regions and disorders. (**A**) Heatmap depicting −ln proportional rank of each pathway per omic in each brain region across disorders (18 analyses). Within each analysis, pathway proportional rank was calculated based on FDR-adjusted *P* divided by the number (*n*) of pathways in the analysis. The five most significant pathways per analysis are shown here. GO categories include biological processes (BP), cellular components (CC), and molecular functions (MF). Upward arrows, positive normalized enrichment scores (NES); downward arrows, negative NES; circles, methylation-related entries (direction unknown). The full name of third pathway from the top is "adaptive immune response based on somatic recombination of immune receptors built from immunoglobulin superfamily domains." (**B** to **D**) Boxplots depicting the range of ρ values corresponding to correlations of pathways' logit(*Ps*) between omics (B), regions (C), or traits (D). (**E** and **F**) Bubble plots of CP enrichment in the DEGs (blue-green outline) and DEPs (red outline) in PTSD (E) and MDD (F). A pathway can belong to multiple categories. Points are sized based on $-\log_{10}$ (FDR-adjusted *P*). Shape fill denotes *z* scores. The most significant pathways are labeled: in (E) and (F), * is used to annotate the STAT3 pathway, and #, for HMGB1 signaling. (**G**) Heatmap of URs enriched in DEGs per brain region in both traits. Significant URs (FDR-adjusted $P < 0.05$) were ranked based on absolute *z* scores (*28*), and the first 50 URs for each disorder were selected. The exogenous chemicals and drugs categories were excluded from plotting. Gray color indicates nonexistent data. UR categories are shown on top. PTSD DG did not have significant URs. Abbreviations of non-gene terms: LPS, lipopolysaccharide; E2, β-estradiol; Ig, immunoglobulin. (**H**) Heatmap of the TF binding enrichment ($-\log_{10}$ FET *P*). Not all analyses showed significant enrichments; # and *, FDR-adjusted $P < 0.05$.

distributed across brain regions (394 in CeA, 441 in DG, 1239 in mPFC, and 292 in all regions). We prioritized top genes from this pool based on at least one of the three following criteria: i) multiregion, ii) multiomic, and iii) multitrait overlap. This qualified 367 genes, henceforth called "top genes" (table S5B). Among the top genes, 280 were associated with PTSD (fig. S5A), 360 with MDD (fig. S5B), and 273 were shared. Gene breakdown per criterion can be found in (*28*) (fig. S5, C to D). PTSD and MDD top genes were significantly enriched in replicated genes (FET, $P = 2.34 \times 10^{-11}$ and 1.04×10^{-21}, respectively).

Following an analogous procedure, we identified 2330 top pathways (2040 in PTSD, 2293 in MDD, 2003 shared; table S5C). Seven top genes (*EDN1*, *FGF2*, *IL1B*, *RAC1*, *TGFB2*, *TGFBR1*, and *STAT3)* were represented in an outlying number of PTSD top pathways, and five (*EDN1*, *FGF2*, *IL1B*, *RAC1*, and *TGFB2*) were represented in MDD top pathways (table S5D).

PTSD and MDD top genes were enriched in GC-associated DEGs (FET, $P = 3.54 \times 10^{-24}$ and 2.41×10^{-32}, respectively) identified in induced pluripotent stem cell (iPSC)–derived neurons after a 4-hour treatment with GR agonist, dexamethasone (DEX) (*24*). Using data from iPSC-derived cerebral organoids treated for 12 hours with DEX (*30*), we found PTSD and MDD top genes' enrichment in DEX-associated DEGs of nonneural progenitors (FET, $P = 3.10 \times 10^{-9}$ and 9.67×10^{-11}, respectively), neural progenitors (FET, $P = 1.40 \times 10^{-8}$ and 1.19×10^{-10}, respectively), and neurons (FET, $P = 5.18 \times 10^{-3}$ and 4.42×10^{-3}, respectively) (table S5E) from our top genes in GR signaling, shedding light on their roles across cell types.

Multiregion, multiomic views

Multiomics factor analysis [MOFA (*31*)] (Fig. 5A) reduced dimensionality by inferring 30 latent factors that captured variance (R^2) of the three omic layers from every brain region (nine views). We observed factors focusing on (i) a single view, namely factor 1 on mPFC methylome and factors 5 to 7 on CeA, DG, and mPFC proteomes, respectively; (ii) a single-omic view in multiple regions, such as factor 2 capturing variance for transcriptome across brain regions; and (iii) multiomic views within one region, including factor 15 on CeA and factor 17 on DG (Fig. 5B). Notably, factor 13 was the only factor with high R^2 values across all nine views, and it showed strong correlation with age (Fig. 5C). This factor may be a multiregion, multiomic "clock." Factor 13 scores differed between diagnoses (*F* test, $P < 9.88 \times 10^{-5}$;

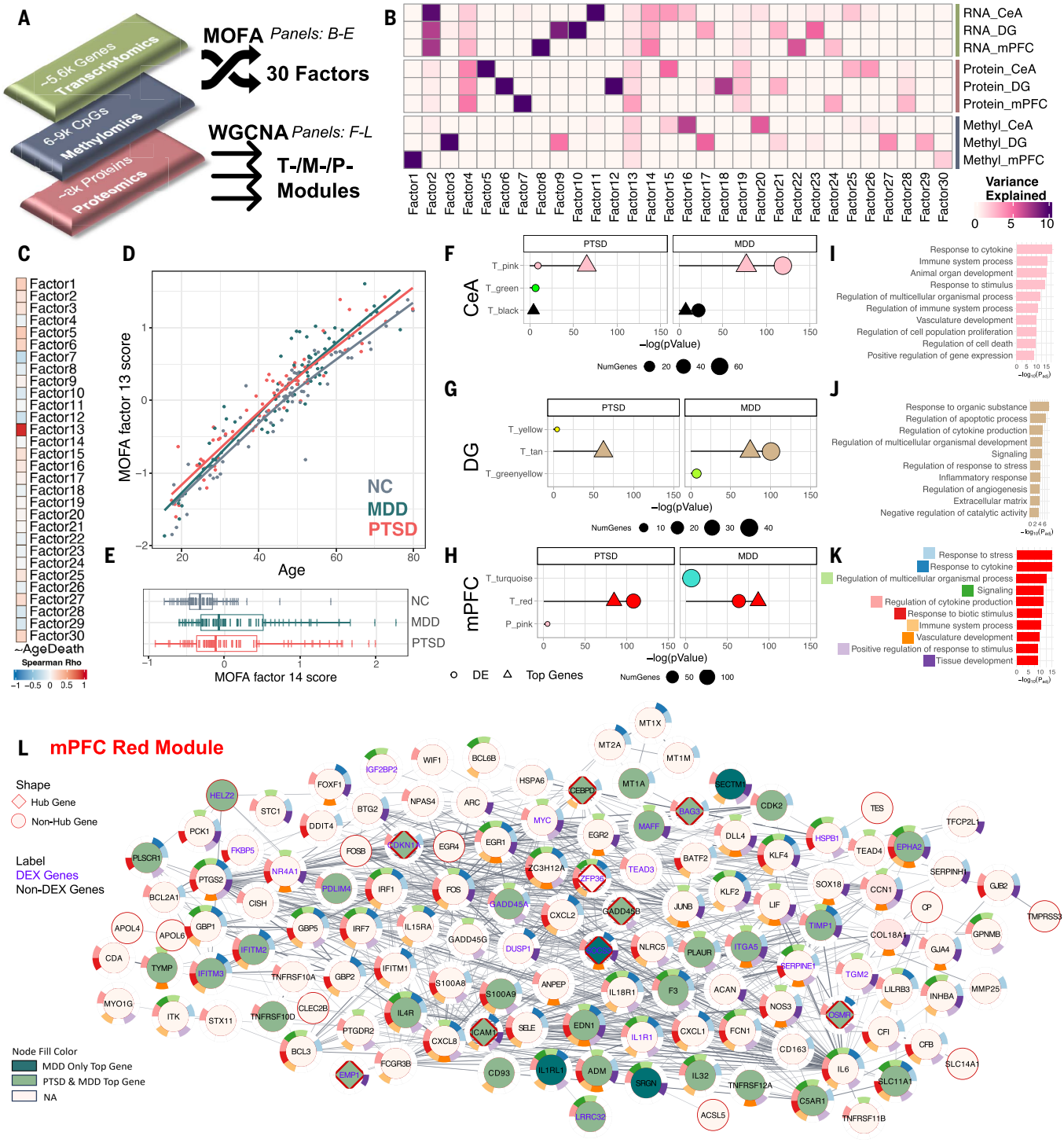

Fig. 5. Multiregion, multiomic integration. (**A**) Nine (three × three) views provided by transcriptomic (T-), methylomic (M-), and proteomic (P-) profiles of each brain region were integrated into thirty latent factors by using MOFA. We used the same input to additionally create coexpression modules for each omic type across brain region using WGCNA. (**B**) Heatmap of variance explained in each of the nine views by each MOFA factor. (**C**) Coefficients of correlation (ρ) of MOFA factors' scores with age at death. (**D**) Scatterplot of MOFA factor 13 scores (*y* axis) with age at death (*x* axis). Locally estimated scatterplot smoothing trendlines are fitted within the diagnosis group. (**E**) Box-and-whisker plots of MOFA factor 14 scores by diagnostic group: data are represented as median ± 1.5 interquartile range (IQR). Individual factor 14 scores are indicated by vertical line markers. In (D) and (E), gray color is used for NCs, blue-green for MDD, and red for PTSD. (**F** to **H**) For three transcriptomic and/or proteomic features per brain region, the enrichment of the respective differentially expressed (DE) features from the PTSD and MDD analyses as well as of the top PTSD and MDD genes (top genes) is depicted [(F) CeA; (G) DG; (H) mPFC]. The *x* axis represents the enrichment significance ($-\log_{10}P$), the size of the point denotes the number of features enriched, and the shape the gene set under interrogation in each analysis (DE, circle; top genes, triangle). (**I** to **K**) The 10 most significant GO terms (color coded) associated with the CeA-pink (I), DG-tan (J), and mPFC-red (K) modules. (**L**) PPI network of the mPFC-red module. The nodes are filled in green if the protein is a PTSD and/or MDD top gene, and the shape of the node indicates whether it is a hub gene (diamond). DEX genes are annotated in purple. Ten GO terms are shown as partially filled donuts around each node according to (K).

Tukey's post-hoc $P < 0.001$ for each group versus NC) (Fig. 5D), which suggests a "multiomic age acceleration" associated with MDD and PTSD. Factor 14 captured the transcriptome of all brain regions, with scores higher in both disorders compared with that of NCs (*F* test, $P < 1.24 \times 10^{-5}$; Tukey's post-hoc $P < 0.001$ for each group versus NCs) (Fig. 5E) and with the factor loadings having moderate correlations with DGE effect sizes (fig. S6A).

Next, we used weighted gene coexpression network analysis (WGCNA) (Fig. 5A) to investigate gene network correlates of MOFA factors. In NC samples, we constructed modules at every omic level per region (table S6A). We highlighted three modules from each region enriched in disease-associated features and top genes (Fig. 5, F to H). The modules (CeA-pink, DG-tan, and mPFC-red) with lowest enrichment *P* values also had the strongest association with factor 14 (fig. S6B). Functional annotation of these modules showed shared immune system processes, inflammatory response, and vasculature development– or angiogenesis-related pathways (Fig. 5, I to K, and table S6B). Notably, the mPFC-red module was associated with response to stress and GCs and exhibited the most significant enrichment with GC-responsive genes (33/181; FET, FDR-adjusted $P = 1.47 \times 10^{-19}$; table S6C), including *FKBP5*. Protein-protein interaction (PPI) network visualization of the three modules (Fig. 5L and fig. S6, C and D) emphasized their hub gene (table S6D) enrichments in both PTSD (FET, $P = 8.48 \times 10^{-24}$) and MDD top genes (FET, $P = 1.60 \times 10^{-27}$).

Single-cell transcriptomics

To explore cell type–specific transcriptional signatures in both disorders, snRNA-seq data from 118 subjects were analyzed [single-cell cohort 1, "Sc.1" (*24*); single-cell cohort 2, "Sc.2 (*25*)] (Fig. 6A and table S7A). As described (*24*), Sc.1 batch 1 contained 362,996 nuclei post quality control (Fig. 6B), and Sc.1 batch 2, 137,230 nuclei (Fig. 6C), clustering in eight broad cell types [excitatory (Ex) and inhibitory (In) neurons, astrocytes (Astro), microglia (Micro), oligodendrocytes (Oligo), oligodendrocyte-precursor cells (OPC), endothelial cells (Endo), and pericytes (Per)] and several subtypes (fig. S7, A and B). Cell subtype annotation similarities between the Sc.1 batches were confirmed (fig. S7, C and D and table S7B-1). Sc.1 batch1 clustering annotations were projected on Sc.2 (~160,000 nuclei), and ~35,000 nuclei were removed because of displaying ambiguous neuronal or non–neuronal profiles. The remaining 125,890 nuclei were reannotated with the Sc.1 batch 1 cell subtype labels (Fig. 6D; fig. S7, E and F; and table S7B-2). Further, we compared cell type proportions of each disorder across the relevant batches (table S7C, -1 and -2) and reported differences in Micro and OPC in MDD (table S7C-3) [supplementary text (*28*)].

We performed batch-level cell type–specific DGE analysis, adjusting for confounders (*28*), followed by meta-analysis. For PTSD, the meta-analysis of the broad cell types contained data from 16 PTSD and 16 NCs (table S8A). On the basis of the batch-specific nuclei contribution to each cell type in Sc.2 (fig. S7F), we meta-analyzed all batches for Astro, Ex, In, and OPC (52 MDD and 50 NCs; table S8B, 1 to 4) and excluded the Sc.2 male batch from the meta-analysis of Endo, Micro, and Oligo (35 MDD and 34 NCs; table S8B, 5 to 7).

In PTSD, we reported 58 FDR-significant DEGs (Fig. 6E and table S8A), with 79% in Ex (46), 17% in In (10), and ~3% in Astro (2). Of these 58 DEGs, 31 overlapped with PTSD DEGs identified when only analyzing the Sc.1 cohort (*24*) [supplementary text (*28*)]. In MDD, we reported 839 FDR-significant DEGs across six cell types (Fig. 6F and table S8B). Astro had the most DEGs with 376 (45%), followed by Ex (26%, 217) and In (24%, 199). The remaining DEGs were found in Oligo (4%, 39), OPCs (1%, 8) and Endo (<1%, 3). Among the MDD DEGs, 18 overlapped with Chatzinakos *et al.* (*24*), 45 overlapped with Maitra *et al.* (*25*), and 716 were newly reported [supplementary text (*28*)].

Four genes in the PTSD-associated 17q21.31 locus (*6*) were prominent DEGs in neurons and Astro in PTSD (*ARL17B*, *LRRC37A2*, *LINC02210-CRHR1*, and *KANSL1*). *ARL17B* was a DEG in neurons (FDR-adjusted $P < 4.6 \times 10^{-9}$) and Astro (FDR-adjusted $P < 9.9 \times 10^{-4}$) with a consistent marked increase of approximately two log2-fold change. In MDD, we reported up-regulation of *FKBP5*, a GC-responsive gene, in neurons and Oligos, expanding previously reported up-regulation in In neurons (*24*). Further intersecting GC-responsive genes (*26*) with disease-associated cell type–specific DEGs revealed up-regulation of *CDH3*, *TAF1C*, and *SLC16A6* in Ex in PTSD and, among other 66 genes (table S8B), up-regulation of *STAT3* in Oligo and down-regulation of *NR4A1* in Endo and Ex in MDD. The multitrait DEGs in the same cell types were limited to down-regulation of *SRSF6*, an alternative splicing regulator and top PTSD gene from the bulk analysis, in Ex and up-regulation of *TMPRSS9* in In.

In PTSD, Ex and In correlated moderately with each other ($\rho = 0.41$) but weakly with glia cell types ($\rho = 0.06$ to 0.26). Endo exhibited no correlation with other cell types (Fig. 6G). In MDD, we detected moderate correlations between neuronal types ($\rho = 0.53$) and with Oligos ($\rho = 0.34$), whereas Astro were moderately correlated with OPCs ($\rho = 0.34$) (Fig. 6H). The between-diagnosis cell type–specific correlation ranged from weak to moderate but was lower than in bulk (mPFC, $\rho = 0.79$), highlighting the importance of studying cell type–specific signals to distinguish pathophysiologically similar disorders (Fig. 6I).

GSEA of cell type–specific PTSD and MDD profiles revealed down-regulated synaptic pathways in neuronal and non-neuronal cell types (table S9A), which were particularly pronounced in MDD Ex neurons, Astro, and Endo (Fig. 6J). Ribosome-related processes were down-regulated in Oligo in both disorders. In MDD, these processes were down-regulated in In neurons, Micro, and OPC, whereas they were up-regulated in Endo and Micro but down-regulated in PTSD Astro. Metabolic and mitochondrial processes were down-regulated in In neurons and Oligo in both disorders and Micro, Oligo, and OPC in MDD. Inflammatory pathways were up-regulated in PTSD and down-regulated in MDD, suggesting differential immune-signaling regulation in each disorder. Furthermore, adhesion and extracellular transport pathways were down-regulated in Astro and Endo in MDD. Notably, glia-related pathways were down-regulated in Micro and Ex neurons in PTSD and In neurons in MDD, whereas they were up-regulated in OPCs in MDD.

We further identified activated cell type–specific URs in MDD (fig. S7G and table S9, B and C). STK11, UR of the stress-activating AMPK pathway, was differentially activated in Astro and neurons. PSEN1 was activated in both In neurons and Astro, whereas APP and TGFB1 were deactivated. CPA confirmed strong deactivation of oxidative phosphorylation and ATP processes in neurons in MDD and mitochondrial dysfunction and Sirtuin signaling pathway activation, especially in In neurons. Non-neuronal cell types involved the inhibition of the stress-hormone complex in Astro, STAT3, and RAC signaling along with the activation of epithelial adherence–related pathways in Oligo and Notch signaling in Endo and OPC (fig. S7H table S9, D and E). PTSD DEGs of In neurons were enriched in THOP1 neuroprotection and the metabolism of amine-derived hormones (including norepinephrine).

Top genes in live blood plasma

To evaluate blood-based biomarkers of PTSD and MDD, we analyzed 1463 plasma proteins in 54,219 UKBB subjects (*32*). PTSD, defined as a binary indicator and a continuous score (~1300), and MDD, defined broadly and strictly (~3500), were compared with healthy subjects (~15,000). We found more FDR-significant proteins associated with MDD compared with PTSD (fig. S8 and table S10A), especially when using the electronic medical record (EMR)–based and help-seeking definitions of MDD. GO pathway analysis of blood DEPs detected ECM organization, response to GCs, various interleukin signaling pathways, neuron projection, and synapse assembly pathways for both disorders (table S10B). FDR-significant CPs and URs for both disorders converged in alterations in transcription regulation and nuclear receptor and cytokine signaling (table S10, C and D).

Blood DEPs' effect sizes had stronger correlations with brain DEGs' effect sizes from all

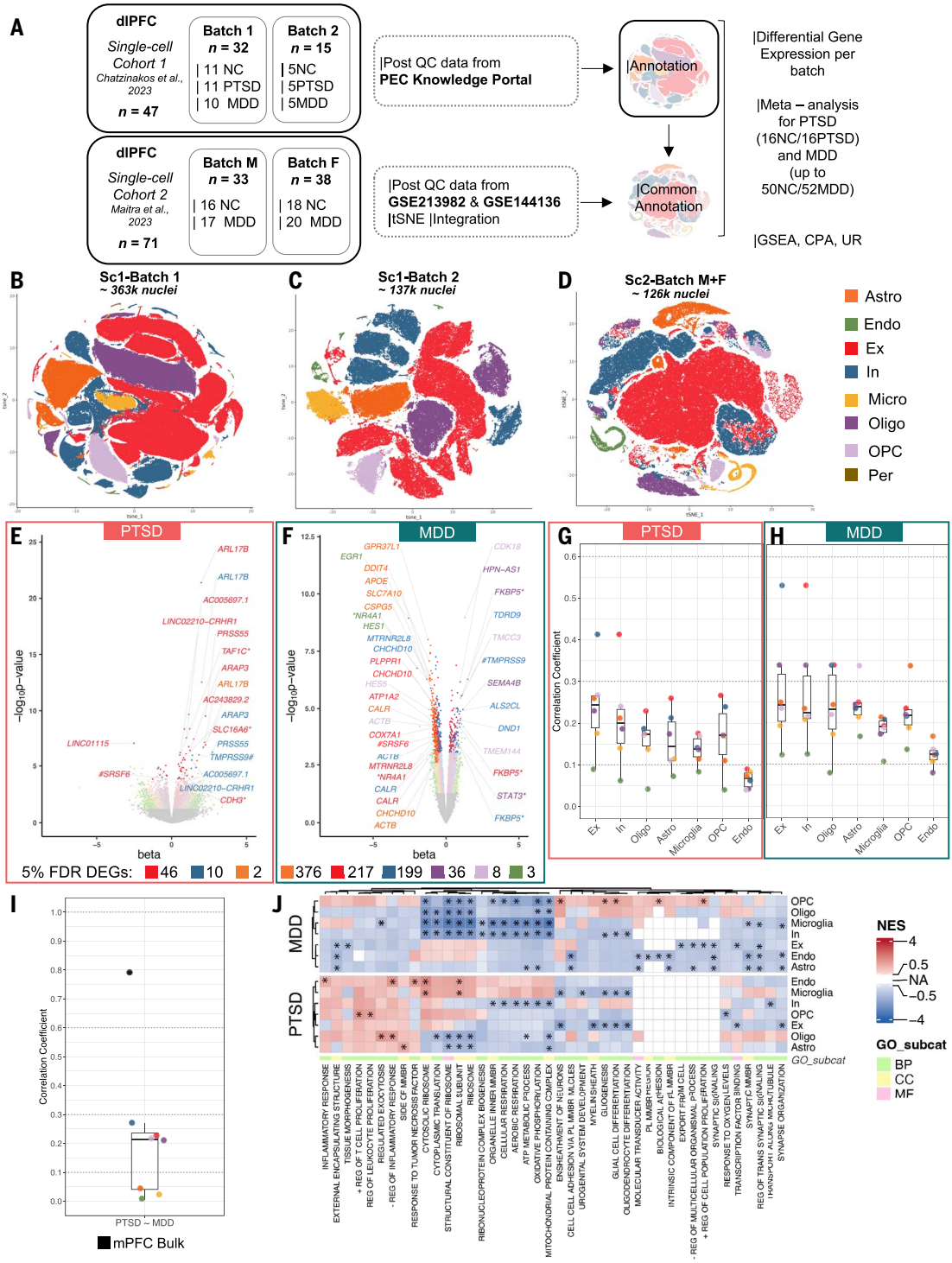

Fig. 6. snRNA-seq study of PTSD, MDD, and NCs in dlPFC. (**A**) Analytic strategy for snRNA-seq datasets. (**B** and **C**) Sc.1 was composed of two batches: batch 1 with 362,996 (B) and batch 2 with 137,230 nuclei (C). Representative tSNE plots of the eight broad cell types are shown. (**D**) tSNE plot of 125,890 nuclei from the two integrated batches of Sc.2 (male and female batches included) annotated to match the identity of the clustering from S.c1. (**E** and **F**) Volcano plots of the DGE in PTSD (E) and MDD (F) across seven cell types (color coded). The dots are colored to denote nominally significant genes ($P < 0.05$) in the respective cell types, and the darker colored dots represent genes with FDR-adjusted $P < 0.05$. Up to five of the most significant (FDR-adjusted $P < 0.05$) cell type–specific DEGs per direction of regulation are labeled along with GC-responsive (*) and PTSD-MDD shared DEGs (#). The number of DEGs passing 5% FDR level per cell type is shown below. (**G** and **H**) Correlation of the DGE effect sizes between cell types in PTSD (G) and MDD (H). Data are represented as median ± 1.5 IQR, whereas the individual points denote the correlation for each cell type. (**I**) Correlation of the cell type–specific DGE effect sizes between PTSD and MDD. Data are represented as median ± 1.5 IQR, whereas the individual points denote the correlation for each cell type. The black dot annotates the correlation of PTSD and MDD in the bulk mPFC tissue. In (G) and (I), horizontal dotted lines denote minimal ($\rho < 0.1$), moderate ($0.3 < \rho < 0.6$), and high ($\rho > 0.6$) correlation. (**J**) Heatmap demonstrating the five most significantly enriched GO pathways in each cell type per disorder. The terms have been clustered based on their NES. The color gradient denotes negative to positive enrichment and the asterisk-annotated pathways have an FDR-adjusted $P < 0.05$. GO categories used included BP, CC, and MF.

brain regions compared with the correlations with brain DEP effect sizes, with the strongest detected between MDD (EMR-based) blood DEPs and MDD or PTSD CeA DEGs (fig. S9). Notably, the EMR-based diagnosis was comparable to the definition of MDD and PTSD from postmortem medical records. PTSD and MDD top genes were enriched in PTSD blood DEPs (24 genes, FET $P = 3.91 \times 10^{-16}$) and MDD blood DEPs (52 genes, FET $P = 1.26 \times 10^{-28}$), respectively (fig. S10A and table S10E-1), with 23 shared across the two disorders in brain and blood. Out of these 23, 19 were multiregion top genes, including *EPHA2* and *TNFRSF1A/12A*. Among the 29 top genes that exclusively overlapped in MDD blood and MDD brain, 22 were multiregion [supplementary text (*28*)].

Forty-three PTSD-associated GO pathways in the brain overlapped with pathways in blood (fig. S10B and table S10E-2), whereas 121 pathways in the MDD brain overlapped with MDD blood [supplementary text (*28*)]. Twenty-two pathways in brain and blood for both disorders related to lipid processes, immune response, and corticosteroid response. The majority were RNA-derived in brain (95% in PTSD, 69% in MDD). Twenty-one pathways, exclusively overlapping in PTSD brain and PTSD blood, were RNA-derived in the brain and included those related to neuroinflammatory response and ECM organization. Of 99 pathways that exclusively overlapped in MDD brain and blood, 31 that included synapse process and axonal guidance originated from methylation in brain.

We noticed that certain pathways, such as axonal guidance, were detected in both brain and blood, involving one omic layer of brain molecular data, whereas their gene members shared between the brain and blood could implicate another brain omic layer.

Brain RNA–based CPs showed overlap with blood CPs. Twelve pathways exhibited multitrait characteristics in both blood protein and brain RNA and protein, including hepatic fibrosis cell activation and LXR and RXR regulation (fig. S10C and table S10E-3). Furthermore, we observed enrichment of brain with blood URs in MDD (fig. S10D and table S10E-4) without substantial overlap of URs in PTSD across brain and blood [details in supplementary text (*28*)].

Multiregion, multiomic view of risk genes and pathways

We estimated that PTSD and MDD GWAS single nucleotide polymorphism (SNP)–based heritability were highly correlated [genetic correlation $R_g = 0.887 \pm 0.013$; methods (*28*)]. Polygenic risk scores (PRS) for each disorder were calculated for 304 subjects across Disc.1, Disc.2, and Rep.1 cohorts. Compared with MDD-PRS, the PTSD-PRS had higher associations with both diagnoses in the respective target population (fig. S11) (*28*).

Fine-mapping of the latest GWAS identified 76 PTSD loci with 68 having one to three credible sets each, and 98 MDD loci with 92 having 1 to 10 credible sets each (tables S11A, -1 and -2, and S11B, -1 and -2, respectively). Local heritability calculations revealed loci in PTSD and MDD that exhibited significant heritability for both disorders (tables S11A, -3 and -4, and S11B, -3 and -4). We observed variability in local genetic correlations as well, particularly with loci involving the 6p22.1/22.2, 17q21.31, and 22q13.1 cytogenetic bands, with the lowest correlations (fig. S12). More details can be found in supplementary text (*28*).

We used quantitative trait locus (xQTL) panels to conduct transcriptomic, methylomic, and proteomic summary-based mendelian randomization (xSMR: TSMR, MSMR, and PSMR, respectively; fig. S13 and table S11C), as well as SNP-based multiomic imputation to conduct transcriptome-, methylome-, and proteome-wide association studies (xWAS: TWAS, MWAS, and PWAS, respectively; fig. S14 and table S11D). PFC-based TSMR and TWAS revealed more PTSD and MDD risk genes compared with AMY- or HIP-based analyses (PTSD, fig. S13, A and B; MDD, fig. S14, A and B), which was consistent with our bulk RNA-seq results. TSMR and TWAS analyses discovered more risk genes than methylomic- and proteomic-based analyses (PTSD, fig. S13, C and D; MDD, fig. S14, C and D). More details can be found in supplementary text (*28*).

We detected intersection of 36 TSMR- and TWAS-based PTSD risk genes and the respective DEGs, 10 of which were top genes (Fig. 7A). Similarly, 31 mPFC and 3 DG TSMR- and TWAS-based MDD risk genes overlapped with respective DEGs (FET, $P = 5.22 \times 10^{-6}$), 6 of which were top genes (Fig. 7B). Only five risk genes of each trait with multiregion, multiomic, and/or multitrait characteristics overlapped with the respective top genes (PTSD, fig. S13E; MDD, fig. S14E).

Using a TWAS pathway method (*33*), we detected TWAS pathways for all three tissues and PWAS pathways for PFC (table S11E, 1 and 2). Contrary to the xWAS gene analysis, HIP had the most risk pathways for both disorders (292 and 551, respectively) compared with AMY (11 and 14, respectively) and PFC (77 and 102, respectively). Pathways shared between brain regions (PTSD, 23, fig. S13F; MDD, 32, fig. S14F) were mostly neural- or neuronal-, trafficking-, organelle-, and metabolism-related. Neuronal and synaptic pathways were overlapping in TWAS and PWAS of both disorders (PTSD, 6; MDD, 32).

The overall correlation between risk pathways and respective bulk tissue–based pathways were low (PTSD, range −0.08 to 0.06; MDD, range −0.1 to 0.13). Immune, synaptic, and developmental pathways were shared between risk and disease process pathway sets (Fig. 7, C to D). Notably, DG RNA gene pathways were significantly enriched in HIP TWAS pathways in both disorders (PTSD, FET $P = 3.08 \times 10^{-2}$, MDD: FET $P = 1.99 \times 10^{-10}$), with 46/48 found in PTSD and 179/180 in MDD top pathways.

Molecular outcomes of gene-by-environment interactions and molecular mediation of risk

We investigated the molecular impact of SNP-by-childhood trauma interactions on TSMR-identified SNP-gene pairs [methods (*28*)]. In PTSD (fig. S15A table S11-F1), many cis–expression quantitative trait loci (eQTLs) effects passed an FDR 5% significance level (61/138 in mPFC, 21/30 in DG, and 19/27 in CeA]. Only rs62060768 (not part of a credible set of 17q21.31) showed an FDR-significant interaction effect on DG *LRRC37A4P* expression, and the same interaction nominally affected CeA *LRRC37A4P* expression. There were two additional 17q21.31 SNPs, both within a credible set, with nominal interaction effects. FDR-significant childhood trauma–only effects were seen for mPFC expression of the top gene *LIMK2*. In MDD (fig. S15B and table S11-F2), many cis-eQTLs passed an FDR 5% level (45/146 in mPFC, 12/15 in DG, and 8/9 in CeA]. We observed only five nominal SNP-by-childhood trauma interactions. One of the SNPs in the *LRRC37A4P* CeA analysis was the same as in the PTSD dataset. FDR-significant childhood trauma–only effects were seen for mPFC *LINC00461* and *CNPPD1*.

In the blood plasma dataset, we had power to distinguish the type of abuse and neglect (fig. S16, A and B, and table S11, -F3 and -F4). We observed SNP effects on plasma proteins for many brain-based eQTLs. For the PTSD and MDD genes, we observed childhood trauma effects in plasma for 20 (including *HLA-E* top gene) and 14 genes, respectively.

We explored the mediation effect of gene expression in the SNP-to-diagnosis effects (Fig. 7E and table S11G). We found that four SNP-to-PTSD diagnosis effects were mediated though mPFC expression of *ATP23*, *CYP2D6*, and *ZSCAN29*, as well as CeA expression of *LINC02210*. We also found two mediation effects for MDD diagnosis through mPFC expression of *STAG3L2* and *TIPIN*.

Multi–cell type view of PTSD and MDD risk

Using a brain cell type annotation (*34*), we detected neuronal enrichment of MDD and PTSD risk genes (fig. S17, A and B). We also determined enrichment of risk genes in dlPFC cell type–specific markers of Sc.1. In- and Ex-neuronal and OPC markers were enriched in risk genes of both disorders (fig. S17, C and D), whereas Oligo markers were enriched only in PTSD. Incorporating gene-level statistics with cell-to-cell heterogeneity (*35*), we found a stronger signal of risk genes in Ex and In neurons and OPCs for MDD than PTSD (Fig. 7F). We then conducted single-cell T SMR (scTSMR) for PTSD and MDD at the dlPFC cell type level, finding

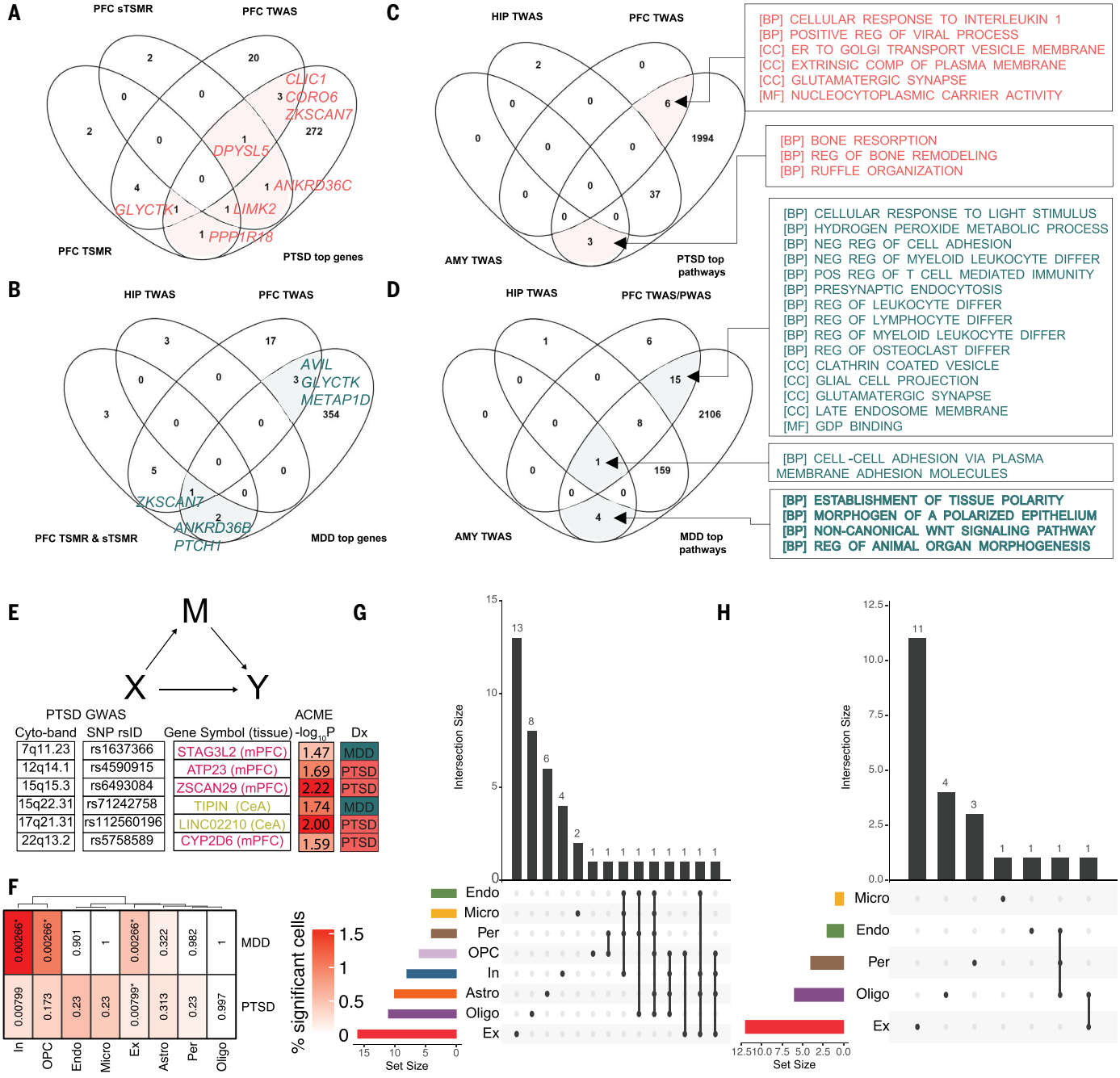

Fig. 7. Identification of GWAS-based risk genes and pathways for PTSD and MDD. (**A** and **B**) Venn diagrams of xSMR- or xWAS-based risk genes overlap-matched with FDR-significant (FDR-adjusted $P < 0.05$) disease process genes and with top genes for PTSD (A) and MDD (B). sTSMR, splicing TSMR. (**C** and **D**) Venn diagrams of xWAS-based risk pathways overlap-matched with FDR-significant (FDR-adjusted $P < 0.05$) disease process pathways and top pathways for PTSD (C) and MDD (D). GO categories used included BP, CC, and MF. (**E**) Heatmap of mediation effects of PTSD or MDD risk genes in the association of GWAS SNPs with diagnosis (Dx) through gene expression alterations. SNP-gene pairs were qualified by brain TSMR analyses of PTSD and MDD GWAS. The first two columns contain the cytogenetic band and the rsID of the qualified GWAS SNP. The mediating gene along with the tissue can be seen in the third column. The $-\log_{10}P$ of the average causal mediation effect (ACME) was the measure of the significance of mediation and is provided as a number and red color intensity. (**F**) Heatmap depicting each cell type–disease association with PTSD and MDD. Numbers indicate FDR-adjusted P of the cell type–disease associations. Heatmap color denotes the proportion (%) of significantly associated cells (FDR-adjusted $P < 0.1$) with the trait. *: FDR-adjusted $P < 0.05$. (**G** and **H**) Upset plots of scTSMR-based risk genes for PTSD (G) and MDD (H) at the level of cell-types in the dlPFC.

cell type–specific risk genes predominantly in Ex neurons and Oligo in both disorders (Fig. 7, G and H, and table S11H, -1 and -2). In PTSD, neuronal PTSD risk genes were significantly enriched in neuronal DEGs (*LINC02210-CRHR1* and *TTC12*, FET $P = 1.92 \times 10^{-3}$), and non-neuronal PTSD risk genes, in non-neuronal DEGs (*ARL17B*, FET $P = 2.69 \times 10^{-3}$). In MDD, only *ANKRD36* overlapped between non-neuronal MDD DEGs and risk genes.

Integration

For full integration, we aggregated and ranked, in tiers of evidence, signals related to top genes across all levels of analyses (table S12A), including (i) PTSD and MDD replication, (ii) membership

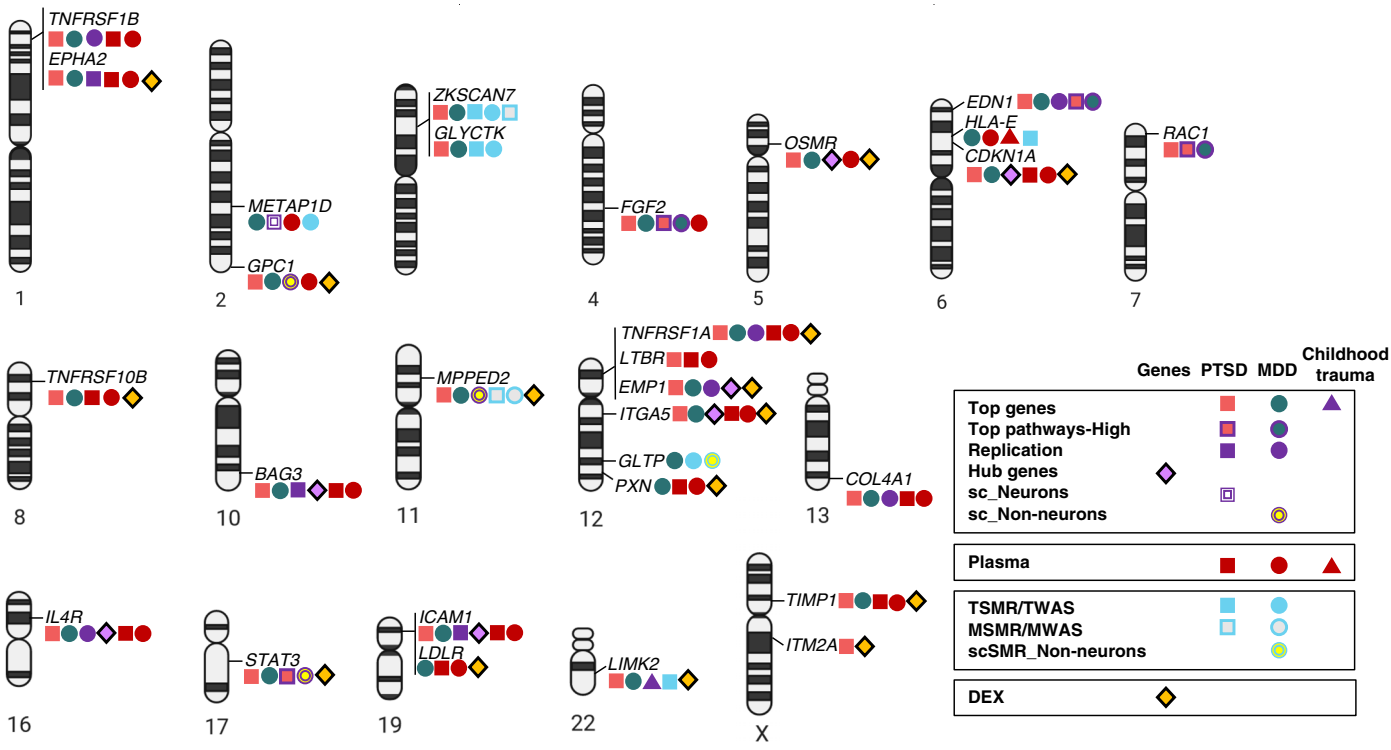

Fig. 8. Integration of results. Top genes were ranked based on accumulating statistical evidence across analyses in tiers (table S12A). Chromosomal locations of top genes with the highest amount evidence are visualized. Six genes are localized on chromosome 12, followed by three genes on chromosome 6. Red squares indicate PTSD top genes, whereas a purple outline indicates membership in PTSD top pathways. Blue-green squares indicate MDD top genes, whereas a purple outline indicates membership in MDD top pathways. Purple squares indicate replication in PTSD analysis, whereas purple circles indicate replication in MDD analysis. Red squares indicate PTSD blood DEPs, and red circles indicate MDD blood DEPs. Purple triangles indicate association with childhood trauma analysis in the brain analyses, whereas red triangles indicate association with childhood trauma in the blood analyses. Purple diamonds indicate genes that are module hubs, whereas yellow diamonds indicate GC regulation (DEX) in iPSC-derived neurons (*26*). Double squares and circles represent single-cell (sc) findings for PTSD and MDD, respectively; neuronal (Neu) versus non-neuronal (NonNeu) distinction is made by the yellow fill (Neu, not filled; NonNeu, filled). In relation to genetic analyses, blue shapes represent TSMR and TWAS, and blue shapes with gray fill represent MSMR and MWAS. The double blue circle with gray fill represents significance in a scTSMR analysis of a non-neuronal cell type.

in top pathways, (iii) acting as hub genes in disease-associated networks, (iv) blood associations, (iv) association with childhood trauma in brain or blood, (vi) snRNA-seq analyses, (vii) brain-based genetic analyses, and (viii) GC regulation. Top genes showed high overlap across these dimensions, which was supported by FDR-significant FET-based enrichments. We visualized the 30 top genes with most convergent evidence (Fig. 8 and fig. S18).

We similarly ranked the top pathways (table S12B) to reveal comparable overlaps and enrichments but with weaker enrichment of plasma pathways and more significant enrichment of cell type–specific pathways. We visualized the top pathways with the most convergent evidence (fig. S19), highlighting the following functional themes: i) neuronal signaling and regulation, ii) immune and inflammatory responses, iii) tissue development and maintenance, and iv) metabolic processes.

Discussion

In this multiregion, multiomic postmortem brain study of PTSD and MDD conducting discovery and replication analyses, we found both shared and distinct molecular signatures in both disorders. The most robust alterations were captured by genes and exons occurring within the mPFC. PTSD had more regional molecular differences than MDD. mDNA changes for PTSD and MDD were mostly localized in the DG and CeA, respectively. Childhood trauma and suicide were the main drivers of signal in both disorders, whereas sex differences were more apparent in MDD. Top genes qualified on the basis of multiregion, multiomic, and/or multitrait importance and by showing robustness through replication, gene networks, snRNA-seq, blood, and/or genetic analyses. Detailed discussions of top genes can be found in the supplementary text (*28*).

Each omic layer implicated distinct biological processes. Notably, we revealed an RNA-based up-regulation, but protein-based down-regulation of immune-related pathways across regions and disorders. These enriched pathways implicated members of the TNF receptor superfamily, namely, the top gene *TNFRSF1A*, which is GC-regulated in neural cells (*24*). IL1β and TNFα, the most prominent URs, are triggered by stress in the brain and periphery (*36*–*38*) and have been previously associated with PTSD and MDD (*8*, *15*, *39*–*42*). Relatedly, the MOFA factor mostly associated with both diagnoses was RNA-based and related to immune RNA modules.

Our multiomic analysis revealed distinct involvement of neuronal and non-neuronal cell types in both disorders. DEGs highlighted immune and ECM pathways, predominantly in non-neuronal external cortical layers and leptomeninges. In MDD, protein alterations were more prominent in neuron-rich deeper layers (*29*), whereas methylation pathway alterations affected neuronal processes in both disorders. Furthermore, our snRNA-seq analysis demonstrated significant transcriptomic changes in both neuronal and non-neuronal cell types, uncovering previously unreported alterations (*23*–*25*). Underlying cell type–specific pathways showed potential in differentiating between the two disorders. Although both disorders exhibited enrichment in neuronal

and non-neuronal cell types, this enrichment appeared more pronounced in MDD. Lastly, scTSMR identified risk genes in Ex neurons and Oligo in both disorders.

Dysregulated ECM-related pathways contained top genes such as *ICAM1* (multiomic in PTSD) and *COL4A1* (multiregion and multiomic in MDD), which were replicated in plasma DEPs. The interstice between ECM and neuronal or synaptic plasticity is covered by axonal guidance molecules such as *EPHA2*, an RNA-based top gene that is replicated and altered in blood and is GC-regulated, which has also been associated with blood-brain barrier (BBB) hyperpermeability (*43*) and suicidality (*44*). Stress-induced BBB hyperpermeability (*45*, *46*) would allow peripheral inflammation, as detected by our large blood proteomics analysis, to enter brain parenchyma.

The robust correlation between PTSD and MDD in GWAS contrasted with the moderate to weak correlations identified in bulk multiomic and snRNA-seq data. Additionally, the limited overlap in both disorders between the genes and pathways implicated in GWAS and those identified in brain molecular data underscored the disparity between disease risk and underlying disease processes. By contrast, greater overlap was seen between disease-associated genes and pathways in brain and blood. Whereas our brain measurements were independent from blood measurements, animal models of individual stress differences have supported shared effects for some pathways (*47*–*49*). Considering the challenges with accessing antemortem brain tissue to profile the disease in real time, our findings support the development of brain-informed blood biomarkers.

Integrating results from various analyses related to the stress system revealed distinct genetic loci but shared downstream molecular signatures. For example, the 17q21.31 locus, which exhibits one of the lowest correlations between PTSD and MDD, has consistently appeared in PTSD GWAS studies (*6*, *21*), with our fine-mapping pointing to *CRHR1*, among other genes. We discovered indications of mediation involving *LINC02210*, whereas the fusion gene of *LINC02210* with *CRHR1* was identified as a neuronal scTSMR-based risk gene and a neuronal DEG for PTSD.

In MDD, GR-encoding *NR3C1* did not appear in a locus of low correlation between PTSD and MDD but was identified solely as an MDD risk gene in PFC TWAS. GR also emerged as a prominent TF across omics for both disorders, targeting ~20% of the top genes. *FKBP5*, which encodes an inhibitory protein for GR function (*50*, *51*), exhibited DGE in the mPFC for PTSD and in Ex and In neurons and Oligo for MDD. Additionally, it was a gene member of the most prominently disease-associated module in the mPFC.

Furthermore, top gene *STAT3* showed DGE in the CeA and mPFC for both traits and in Oligo for MDD and was involved in several top pathways associated with PTSD related to wound healing, mitochondrial function, inflammation, and synaptic plasticity in neurons (*52*–*54*). STAT3 activation in mPFC was also evident for both disorders. Notably, *STAT3* is GC responsive in iPSC-derived neurons (*26*), acts as a GR coactivator (*55*), and has recently been linked to depressive-like behavior in animal models (*56*, *57*).

The dynamic interplay between genetic susceptibility and downstream biology evolves across the lifespan. Our investigation unveiled enduring effects of childhood trauma on risk loci linked to both disorders alongside insights into the influence of aging. MDD and PTSD share mechanistic pathways with neurodegenerative conditions (*58*). Notably, the PTSD-associated 17q21.31 locus, including the gene encoding MAPT and MDD-associated *APOE* in Astro, both implicated in neurodegeneration, underscores these connections (*59*). Moreover, factor 13, a multiomic "clock" indicative of age acceleration in stress-related disorders, aligns closely with findings from epigenetic-specific clocks based on blood and brain samples (*60*–*63*).

Study limitations primarily stem from inherent biases in postmortem brain research around population selection (including ancestry), clinical assessment, comorbidities, and end-of-life state. The current large study is constrained in power at variable levels across various molecular modalities, tissues, and cell types. We also did not comprehensively characterize the epigenetic landscape and did not fully capture all cell subtypes and states. The description of our results focused primarily on convergent signals across regions or omics or traits, and ancillary studies could explain signal contrasts across the molecular, biological, and clinical dimensions. Detailed limitations can be found in supplementary text (*28*).

Our data suggest that a systems biology approach is necessary to understand the complexity of molecular alterations in brain circuitry underlying stress-related disorders such as PTSD and MDD. Merging multiomics from multiple brain regions with other molecular data can result in the identification of specific genes and regulatory mechanisms. Capturing these nuances is critical when aiming to develop informative biomarkers and discover potential therapeutic strategies.

Materials and methods summary

The PTSD Brainomics Project (PEC Phase 2) generated a multiomic dataset from the mPFC, DG, and CeA of 231 subjects with PTSD and/or MDD and NCs from two cohorts ($n_{Disc.1}$ = 150, $n_{Disc.2}$ = 81). Samples were i) genotyped with Omni2.5 BeadChip and imputed with TOPMed service; ii) ribo-zero RNA-sequenced with TruSeq v2 and processed with SPEAQeasy (*64*) to extract transcriptomic features at gene, exon, splice junction, and transcript levels; iii) methylation profiled with EPIC BeadChip and processed with minifi package (*65*); and iv) protein assayed with tandem mass tag isobaric labeling followed by liquid chromatography coupled to tandem mass spectrometry and proteomic features (proteins and peptides) were searched against UniProt database. Data were normalized and analyses were adjusted for confounds, cell-type proportions, global ancestry, demographics, and clinical characteristics. We assessed the association of diagnosis across omics and regions and conducted subanalyses using the limma package (*66*). Results were meta-analyzed across discovery cohorts [metafor (*67*)]. DMRs were detected with ENmix::comb-p (*68*). We replicated our findings by generating Rep.1 (same genomic features as Disc. cohorts, n = 73) and reanalyzing Rep.2 [contained RNA-seq and mDNA data from a prior study, n = 41 (*14*, *17*)] separately and as a meta-analysis of common features (n = 114).

GSEA was performed with fgsea and methylGSA packages (*69*, *70*). We used ingenuity pathway analysis to identify CPs and URs. For transcription factor–binding enrichment, we used Enrichr (*71*). For spatial registration of disease signatures, we used spatialLIBD (*72*). Multiomic integration of DGE results was performed with MOFA (*31*).

We leveraged publicly available dlPFC snRNA-seq datasets from 118 individuals (*23*–*25*), ensuring cell type and subtype alignment using Seurat (*73*). We analyzed batches separately and then meta-analyzed. Functional annotations were interrogated with GSEA and CP and UR analyses. Protein-based biomarkers were evaluated in plasma from >50,000 UKBB participants (*32*). We performed association testing (limma) and pathway analysis [clusterProfiler (*74*)].

We used the largest available PTSD and MDD GWAS datasets (*5*, *6*). With LDSC (*75*), we estimated global SNP-based heritability and genetic correlation between the disorders, whereas with LAVA (*76*), we estimated local heritability and correlation. For fine mapping, we used a combination of FUMA (*77*) with SusieR (*78*, *79*). GWAS-based risk genes were identified with SMR using bulk-tissue cis-xQTL databases matching the omics and brain regions of our bulk tissue studies (*58*, *80*, *81*) and cell type–specific cis-eQTLs matching the cell types of our snRNA-seq studies (*82*). Risk genes were also identified with xWAS (*83*) [implemented by JEPEGMIX2-P (*33*) with pretrained molecular imputation models (*84*–*86*) matching the omics and brain regions of our bulk tissue studies]. For cell-type enrichment, we used partitioned heritability (*87*, *88*), MAGMA (*89*), and scDRS (*35*). SNP candidates for gene-by-environment interactions were based on the TSMR results. SNP-gene pairs were considered if the target gene existed in our normalized expression dataset of the respective tissues. For

UKBB plasma proteomics, we used the same gene pairs but further reduced it to SNP-protein pairs if the target protein was expressed in plasma. For environment variables, we used childhood trauma. Additive and interaction models were tested. To test mediation effects of gene expression in the SNP-to-diagnosis effects, we used statsmodels (*90*).

Full materials and methods can be found in the supplementary materials (*28*).

REFERENCES AND NOTES

1. J. W. Smoller, The Genetics of Stress-Related Disorders: PTSD, Depression, and Anxiety Disorders. *Neuropsychopharmacology* **41**, 297–319 (2016). doi: 10.1038/npp.2015.266; pmid: 26321314
2. N. R. Wray *et al*., eQTLGen; 23andMe; Major Depressive Disorder Working Group of the Psychiatric Genomics Consortium, Genome-wide association analyses identify 44 risk variants and refine the genetic architecture of major depression. *Nat. Genet.* **50**, 668–681 (2018). doi: 10.1038/s41588-018-0090-3; pmid: 29700475
3. D. M. Howard *et al*., Genome-wide meta-analysis of depression identifies 102 independent variants and highlights the importance of the prefrontal brain regions. *Nat. Neurosci.* **22**, 343–352 (2019). doi: 10.1038/s41593-018-0326-7; pmid: 30718901
4. N. Cai *et al*., Minimal phenotyping yields genome-wide association signals of low specificity for major depression. *Nat. Genet.* **52**, 437–447 (2020). doi: 10.1038/s41588-020-0594-5; pmid: 32231276
5. D. F. Levey *et al*., Bi-ancestral depression GWAS in the Million Veteran Program and meta-analysis in >1.2 million individuals highlight new therapeutic directions. *Nat. Neurosci.* **24**, 954–963 (2021). doi: 10.1038/s41593-021-00860-2; pmid: 34045744
6. C. M. Nievergelt *et al*., Discovery of 95 PTSD loci provides insight into genetic architecture and neurobiology of trauma and stress-related disorders. *Nat. Genet.* (2024). doi: 10.1038/s41588-024-01707-9; pmid: 38637617
7. R. Yehuda *et al*., Gene expression patterns associated with posttraumatic stress disorder following exposure to the World Trade Center attacks. *Biol. Psychiatry* **66**, 708–711 (2009). doi: 10.1016/j.biopsych.2009.02.034; pmid: 19393990
8. D. Lindqvist *et al*., Proinflammatory milieu in combat-related PTSD is independent of depression and early life stress. *Brain Behav. Immun.* **42**, 81–88 (2014). doi: 10.1016/j.bbi.2014.06.003; pmid: 24929195
9. M. W. Logue *et al*., An analysis of gene expression in PTSD implicates genes involved in the glucocorticoid receptor pathway and neural responses to stress. *Psychoneuroendocrinology* **57**, 1–13 (2015). doi: 10.1016/j.psyneuen.2015.03.016; pmid: 25867994
10. M. S. Breen *et al*., PTSD Blood Transcriptome Mega-Analysis: Shared Inflammatory Pathways across Biological Sex and Modes of Trauma. *Neuropsychopharmacology* **43**, 469–481 (2018). doi: 10.1038/npp.2017.220; pmid: 28925389
11. A. K. Smith *et al*., VA Mid-Atlantic MIRECC Workgroup; PGC PTSD Epigenetics Workgroup, Epigenome-wide meta-analysis of PTSD across 10 military and civilian cohorts identifies methylation changes in AHRR. *Nat. Commun.* **11**, 5965 (2020). doi: 10.1038/s41467-020-19615-x; pmid: 33235198
12. M. Bekhbat *et al*., Transcriptomic signatures of psychomotor slowing in peripheral blood of depressed patients: Evidence for immunometabolic reprogramming. *Mol. Psychiatry* **26**, 7384–7392 (2021). doi: 10.1038/s41380-021-01258-z; pmid: 34535767
13. S. Katrinli *et al*., Epigenome-wide meta-analysis of PTSD symptom severity in three military cohorts implicates DNA methylation changes in genes involved in immune system and oxidative stress. *Mol. Psychiatry* **27**, 1720–1728 (2022). doi: 10.1038/s41380-021-01398-2; pmid: 34992238
14. M. I. Mighdoll *et al*., Implementation and clinical characteristics of a posttraumatic stress disorder brain collection. *J. Neurosci. Res.* **96**, 16–20 (2018). doi: 10.1002/jnr.24093; pmid: 28609565
15. M. W. Logue *et al*., Gene expression in the dorsolateral and ventromedial prefrontal cortices implicates immune-related gene networks in PTSD. *Neurobiol. Stress* **15**, 100398 (2021). doi: 10.1016/j.ynstr.2021.100398; pmid: 34646915
16. M. J. Girgenti *et al*., Transcriptomic organization of the human brain in post-traumatic stress disorder. *Nat. Neurosci.* **24**, 24–33 (2021). doi: 10.1038/s41593-020-00748-7; pmid: 33349712
17. A. E. Jaffe *et al*., Decoding Shared Versus Divergent Transcriptomic Signatures Across Cortico-Amygdala Circuitry in PTSD and Depressive Disorders. *Am. J. Psychiatry* **179**, 673–686 (2022). doi: 10.1176/appi.ajp.21020162; pmid: 35791611
18. M. W. Logue *et al*., An epigenome-wide association study of posttraumatic stress disorder in US veterans implicates several new DNA methylation loci. *Clin. Epigenetics* **12**, 46 (2020). doi: 10.1186/s13148-020-0820-0; pmid: 32171335
19. E. J. Wolf *et al*., Gene expression correlates of advanced epigenetic age and psychopathology in postmortem cortical tissue. *Neurobiol. Stress* **15**, 100371 (2021). doi: 10.1016/j.ynstr.2021.100371; pmid: 34458511
20. L. M. Huckins *et al*., Analysis of Genetically Regulated Gene Expression Identifies a Prefrontal PTSD Gene, SNRNP35, Specific to Military Cohorts. *Cell Rep.* **31**, 107716 (2020). doi: 10.1016/j.celrep.2020.107716; pmid: 32492425
21. M. B. Stein *et al*., Genome-wide association analyses of posttraumatic stress disorder and its symptom subdomains in the Million Veteran Program. *Nat. Genet.* **53**, 174–184 (2021). doi: 10.1038/s41588-020-00767-x; pmid: 33510476
22. N. Matosin *et al*., Associations of psychiatric disease and ageing with FKBP5 expression converge on superficial layer neurons of the neocortex. *Acta Neuropathol.* **145**, 439–459 (2023). doi: 10.1007/s00401-023-02541-9; pmid: 36729133
23. C. Nagy *et al*., Single-nucleus transcriptomics of the prefrontal cortex in major depressive disorder implicates oligodendrocyte precursor cells and excitatory neurons. *Nat. Neurosci.* **23**, 771–781 (2020). doi: 10.1038/s41593-020-0621-y; pmid: 32341540
24. C. Chatzinakos *et al*., Single-Nucleus Transcriptome Profiling of Dorsolateral Prefrontal Cortex: Mechanistic Roles for Neuronal Gene Expression, Including the 17q21.31 Locus, in PTSD Stress Response. *Am. J. Psychiatry* **180**, 739–754 (2023). doi: 10.1176/appi.ajp.20220478; pmid: 37491937
25. M. Maitra *et al*., Cell type specific transcriptomic differences in depression show similar patterns between males and females but implicate distinct cell types and genes. *Nat. Commun.* **14**, 2912 (2023). doi: 10.1038/s41467-023-38530-5; pmid: 37217515
26. K. R. Dean *et al*., Multi-omic biomarker identification and validation for diagnosing warzone-related post-traumatic stress disorder. *Mol. Psychiatry* **25**, 3337–3349 (2020). doi: 10.1038/s41380-019-0496-z; pmid: 31501510
27. S. Dalvie *et al*., From genetics to systems biology of stress-related mental disorders. *Neurobiol. Stress* **15**, 100393 (2021). doi: 10.1016/j.ynstr.2021.100393; pmid: 34584908
28. See supplementary materials.
29. L. A. Huuki-Myers *et al*., A data-driven single-cell and spatial transcriptomic map of the human prefrontal cortex. *Science* **384**, eadh1938 (2024). doi: 10.1126/science.adh1938
30. C. Cruceanu *et al*., Cell-Type-Specific Impact of Glucocorticoid Receptor Activation on the Developing Brain: A Cerebral Organoid Study. *Am. J. Psychiatry* **179**, 375–387 (2022). doi: 10.1176/appi.ajp.2021.21010095; pmid: 34698522
31. R. Argelaguet *et al*., Multi-Omics Factor Analysis-a framework for unsupervised integration of multi-omics data sets. *Mol. Syst. Biol.* **14**, e8124 (2018). doi: 10.15252/msb.20178124; pmid: 29925568
32. B. B. Sun *et al*., Plasma proteomic associations with genetics and health in the UK Biobank. *Nature* **622**, 329–338 (2023). doi: 10.1038/s41586-023-06592-6; pmid: 37794186
33. C. Chatzinakos *et al*., TWAS pathway method greatly enhances the number of leads for uncovering the molecular underpinnings of psychiatric disorders. *Am. J. Med. Genet. B. Neuropsychiatr. Genet.* **183**, 454–463 (2020). doi: 10.1002/ajmg.b.32823; pmid: 32954640
34. J. D. Cahoy *et al*., A transcriptome database for astrocytes, neurons, and oligodendrocytes: A new resource for understanding brain development and function. *J. Neurosci.* **28**, 264–278 (2008). doi: 10.1523/JNEUROSCI.4178-07.2008; pmid: 18171944
35. M. J. Zhang *et al*., Polygenic enrichment distinguishes disease associations of individual cells in single-cell RNA-seq data. *Nat. Genet.* **54**, 1572–1580 (2022). doi: 10.1038/s41588-022-01167-z; pmid: 36050550
36. J. D. Johnson, D. F. Barnard, A. C. Kulp, D. M. Mehta, Neuroendocrine Regulation of Brain Cytokines After Psychological Stress. *J. Endocr. Soc.* **3**, 1302–1320 (2019). doi: 10.1210/js.2019-00053; pmid: 31259292
37. A. L. Marsland, C. Walsh, K. Lockwood, N. A. John-Henderson, The effects of acute psychological stress on circulating and stimulated inflammatory markers: A systematic review and meta-analysis. *Brain Behav. Immun.* **64**, 208–219 (2017). doi: 10.1016/j.bbi.2017.01.011; pmid: 28089638
38. K. A. Jones, C. Thomsen, The role of the innate immune system in psychiatric disorders. *Mol. Cell. Neurosci.* **53**, 52–62 (2013). doi: 10.1016/j.mcn.2012.10.002; pmid: 23064447
39. C. L. Raison *et al*., A randomized controlled trial of the tumor necrosis factor antagonist infliximab for treatment-resistant depression: The role of baseline inflammatory biomarkers. *JAMA Psychiatry* **70**, 31–41 (2013). doi: 10.1001/2013.jamapsychiatry.4; pmid: 22945416
40. D. Enache, C. M. Pariante, V. Mondelli, Markers of central inflammation in major depressive disorder: A systematic review and meta-analysis of studies examining cerebrospinal fluid, positron emission tomography and post-mortem brain tissue. *Brain Behav. Immun.* **81**, 24–40 (2019). doi: 10.1016/j.bbi.2019.06.015; pmid: 31195092
41. J. J. Yang, W. Jiang, Immune biomarkers alterations in post-traumatic stress disorder: A systematic review and meta-analysis. *J. Affect. Disord.* **268**, 39–46 (2020). doi: 10.1016/j.jad.2020.02.044; pmid: 32158005
42. T. L. Peruzzolo *et al*., Inflammatory and oxidative stress markers in post-traumatic stress disorder: A systematic review and meta-analysis. *Mol. Psychiatry* **27**, 3150–3163 (2022). doi: 10.1038/s41380-022-01564-0; pmid: 35477973
43. V. A. Malik, B. Di Benedetto, The Blood-Brain Barrier and the EphR/Ephrin System: Perspectives on a Link Between Neurovascular and Neuropsychiatric Disorders. *Front. Mol. Neurosci.* **11**, 127 (2018). doi: 10.3389/fnmol.2018.00127; pmid: 29706868
44. A. L. Romero-Pimentel *et al*., Integrative DNA Methylation and Gene Expression Analysis in the Prefrontal Cortex of Mexicans Who Died by Suicide. *Int. J. Neuropsychopharmacol.* **24**, 935–947 (2021). doi: 10.1093/ijnp/pyab042; pmid: 34214149
45. S. Najjar, D. M. Pearlman, O. Devinsky, A. Najjar, D. Zagzag, Neurovascular unit dysfunction with blood-brain barrier hyperpermeability contributes to major depressive disorder: A review of clinical and experimental evidence. *J. Neuroinflammation* **10**, 906 (2013). doi: 10.1186/1742-2094-10-142; pmid: 24289502
46. M. O. Welcome, N. E. Mastorakis, Stress-induced blood brain barrier disruption: Molecular mechanisms and signaling pathways. *Pharmacol. Res.* **157**, 104769 (2020). doi: 10.1016/j.phrs.2020.104769; pmid: 32275963
47. N. P. Daskalakis, H. Cohen, G. Cai, J. D. Buxbaum, R. Yehuda, Expression profiling associates blood and brain glucocorticoid receptor signaling with trauma-related individual differences in both sexes. *Proc. Natl. Acad. Sci. U.S.A.* **111**, 13529–13534 (2014). doi: 10.1073/pnas.1401660111; pmid: 25114262
48. A. Lori *et al*., Dynamic Patterns of Threat-Associated Gene Expression in the Amygdala and Blood. *Front. Psychiatry* **9**, 778 (2019). doi: 10.3389/fpsyt.2018.00778; pmid: 30705647
49. G. E. Hodes *et al*., Individual differences in the peripheral immune system promote resilience versus susceptibility to social stress. *Proc. Natl. Acad. Sci. U.S.A.* **111**, 16136–16141 (2014). doi: 10.1073/pnas.1415191111; pmid: 25331895
50. J. Hartmann *et al*., Mineralocorticoid receptors dampen glucocorticoid receptor sensitivity to stress via regulation of FKBP5. *Cell Rep.* **35**, 109185 (2021). doi: 10.1016/j.celrep.2021.109185; pmid: 34077736
51. E. B. Binder, The role of FKBP5, a co-chaperone of the glucocorticoid receptor in the pathogenesis and therapy of affective and anxiety disorders. *Psychoneuroendocrinology* **34** (Suppl 1), S186–S195 (2009). doi: 10.1016/j.psyneuen.2009.05.021; pmid: 19560279
52. E. J. Hillmer, H. Zhang, H. S. Li, S. S. Watowich, STAT3 signaling in immunity. *Cytokine Growth Factor Rev.* **31**, 1–15 (2016). doi: 10.1016/j.cytogfr.2016.05.001; pmid: 27185365
53. R. J. Antonia *et al*., STAT3 regulates inflammatory cytokine production downstream of TNFR1 by inducing expression of TNFAIP3/A20. *J. Cell. Mol. Med.* **26**, 4591–4601 (2022). doi: 10.1111/jcmm.17489; pmid: 35841281
54. C. S. Nicolas *et al*., The role of JAK-STAT signaling within the CNS. *JAK-STAT* **2**, e22925 (2013). doi: 10.4161/jkst.22925; pmid: 24058789
55. Z. Zhang, S. Jones, J. S. Hagood, N. L. Fuentes, G. M. Fuller, STAT3 acts as a co-activator of glucocorticoid receptor signaling. *J. Biol. Chem.* **272**, 30607–30610 (1997). doi: 10.1074/jbc.272.49.30607; pmid: 9388192
56. S. H. Kwon *et al*., Dysfunction of Microglial STAT3 Alleviates Depressive Behavior via Neuron-Microglia Interactions.

Neuropsychopharmacology **42**, 2072–2086 (2017). doi: 10.1038/npp.2017.93; pmid: 28480882
57. W. Y. Chen *et al*., Transcriptomics identifies STAT3 as a key regulator of hippocampal gene expression and anhedonia during withdrawal from chronic alcohol exposure. *Transl. Psychiatry* **11**, 298 (2021). doi: 10.1038/s41398-021-01421-8; pmid: 34016951
58. T. S. Wingo *et al*., Shared mechanisms across the major psychiatric and neurodegenerative diseases. *Nat. Commun.* **13**, 4314 (2022). doi: 10.1038/s41467-022-31873-5; pmid: 35882878
59. N. V. Harerimana, A. M. Goate, K. R. Bowles, The influence of 17q21.31 and *APOE* genetic ancestry on neurodegenerative disease risk. *Front. Aging Neurosci.* **14**, 1021918 (2022). doi: 10.3389/fnagi.2022.1021918; pmid: 36337698
60. M. P. Boks *et al*., Longitudinal changes of telomere length and epigenetic age related to traumatic stress and post-traumatic stress disorder. *Psychoneuroendocrinology* **51**, 506–512 (2015). doi: 10.1016/j.psyneuen.2014.07.011; pmid: 25129579
61. E. J. Wolf *et al*., Traumatic stress and accelerated DNA methylation age: A meta-analysis. *Psychoneuroendocrinology* **92**, 123–134 (2018). doi: 10.1016/j.psyneuen.2017.12.007; pmid: 29452766
62. E. J. Wolf *et al*., Klotho, PTSD, and advanced epigenetic age in cortical tissue. *Neuropsychopharmacology* **46**, 721–730 (2021). doi: 10.1038/s41386-020-00884-5; pmid: 33096543
63. R. Yang *et al*., A DNA methylation clock associated with age-related illnesses and mortality is accelerated in men with combat PTSD. *Mol. Psychiatry* **26**, 4999–5009 (2021). doi: 10.1038/s41380-020-0755-z; pmid: 32382136
64. N. J. Eagles *et al*., SPEAQeasy: A scalable pipeline for expression analysis and quantification for R/bioconductor-powered RNA-seq analyses. *BMC Bioinformatics* **22**, 224 (2021). doi: 10.1186/s12859-021-04142-3; pmid: 33932985
65. M. J. Aryee *et al*., Minfi: A flexible and comprehensive Bioconductor package for the analysis of Infinium DNA methylation microarrays. *Bioinformatics* **30**, 1363–1369 (2014). doi: 10.1093/bioinformatics/btu049; pmid: 24478339
66. M. E. Ritchie *et al*., limma powers differential expression analyses for RNA-sequencing and microarray studies. *Nucleic Acids Res.* **43**, e47 (2015). doi: 10.1093/nar/gkv007; pmid: 25605792
67. W. Viechtbauer, Conducting Meta-Analyses inRwith themetaforPackage. *J. Stat. Softw.* **36**, 1–48 (2010). doi: 10.18637/jss.v036.i03
68. Z. Xu, L. Niu, L. Li, J. A. Taylor, ENmix: A novel background correction method for Illumina HumanMethylation450 BeadChip. *Nucleic Acids Res.* **44**, e20 (2016). doi: 10.1093/nar/gkv907; pmid: 26384415
69. G. Korotkevich *et al*., Fast gene set enrichment analysis. *bioRxiv*060012 [Preprint] (2021); .doi: 10.1101/060012
70. X. Ren, P. F. Kuan, methylGSA: A Bioconductor package and Shiny app for DNA methylation data length bias adjustment in gene set testing. *Bioinformatics* **35**, 1958–1959 (2019). doi: 10.1093/bioinformatics/bty892; pmid: 30346483
71. Z. Xie *et al*., Gene Set Knowledge Discovery with Enrichr. *Curr. Protoc.* **1**, e90 (2021). doi: 10.1002/cpz1.90; pmid: 33780170
72. B. Pardo *et al*., spatialLIBD: An R/Bioconductor package to visualize spatially-resolved transcriptomics data. *BMC Genomics* **23**, 434 (2022). doi: 10.1186/s12864-022-08601-w; pmid: 35689177
73. R. Satija, J. A. Farrell, D. Gennert, A. F. Schier, A. Regev, Spatial reconstruction of single-cell gene expression data. *Nat. Biotechnol.* **33**, 495–502 (2015). doi: 10.1038/nbt.3192; pmid: 25867923
74. G. Yu, Q.-Y. He, P. A. Reactome, An R/Bioconductor package for reactome pathway analysis and visualization. *Mol. Biosyst.* **12**, 477–479 (2016). doi: 10.1039/C5MB00663E; pmid: 26661513
75. B. K. Bulik-Sullivan *et al*., LD Score regression distinguishes confounding from polygenicity in genome-wide association studies. *Nat. Genet.* **47**, 291–295 (2015). doi: 10.1038/ng.3211; pmid: 25642630
76. J. Werme, S. van der Sluis, D. Posthuma, C. A. de Leeuw, An integrated framework for local genetic correlation analysis. *Nat. Genet.* **54**, 274–282 (2022). doi: 10.1038/s41588-022-01017-y; pmid: 35288712
77. K. Watanabe, E. Taskesen, A. van Bochoven, D. Posthuma, Functional mapping and annotation of genetic associations with FUMA. *Nat. Commun.* **8**, 1826 (2017). doi: 10.1038/s41467-017-01261-5; pmid: 29184056
78. Y. Zou, P. Carbonetto, G. Wang, M. Stephens, Fine-mapping from summary data with the "Sum of Single Effects" model. *PLOS Genet.* **18**, e1010299 (2022). doi: 10.1371/journal.pgen.1010299; pmid: 35853082
79. G. Wang, A. Sarkar, P. Carbonetto, M. Stephens, A simple new approach to variable selection in regression, with application to genetic fine mapping. *J. R. Stat. Soc. Series B Stat. Methodol.* **82**, 1273–1300 (2020). doi: 10.1111/rssb.12388; pmid: 37220626
80. T. Qi *et al*., Genetic control of RNA splicing and its distinct role in complex trait variation. *Nat. Genet.* **54**, 1355–1363 (2022). doi: 10.1038/s41588-022-01154-4; pmid: 35982161
81. T. Qi *et al*., eQTLGen Consortium, Identifying gene targets for brain-related traits using transcriptomic and methylomic data from blood. *Nat. Commun.* **9**, 2282 (2018). doi: 10.1038/s41467-018-04558-1; pmid: 29891976
82. J. Bryois *et al*., Cell-type-specific cis-eQTLs in eight human brain cell types identify novel risk genes for psychiatric and neurological disorders. *Nat. Neurosci.* **25**, 1104–1112 (2022). doi: 10.1038/s41593-022-01128-z; pmid: 35915177
83. E. R. Gamazon *et al*., A gene-based association method for mapping traits using reference transcriptome data. *Nat. Genet.* **47**, 1091–1098 (2015).
84. A. N. Barbeira *et al*., GTEx Consortium, Exploiting the GTEx resources to decipher the mechanisms at GWAS loci. *Genome Biol.* **22**, 49 (2021). doi: 10.1186/s13059-020-02252-4; pmid: 33499903
85. A. E. Jaffe *et al*., Profiling gene expression in the human dentate gyrus granule cell layer reveals insights into schizophrenia and its genetic risk. *Nat. Neurosci.* **23**, 510–519 (2020). doi: 10.1038/s41593-020-0604-z; pmid: 32203495
86. A. E. Jaffe *et al*., BrainSeq Consortium, Developmental and genetic regulation of the human cortex transcriptome illuminate schizophrenia pathogenesis. *Nat. Neurosci.* **21**, 1117–1125 (2018). doi: 10.1038/s41593-018-0197-y; pmid: 30050107
87. H. K. Finucane *et al*., ReproGen Consortium; Schizophrenia Working Group of the Psychiatric Genomics Consortium; RACI Consortium, Partitioning heritability by functional annotation using genome-wide association summary statistics. *Nat. Genet.* **47**, 1228–1235 (2015). doi: 10.1038/ng.3404; pmid: 26414678
88. H. K. Finucane *et al*., Heritability enrichment of specifically expressed genes identifies disease-relevant tissues and cell types. *Nat. Genet.* **50**, 621–629 (2018).
89. C. A. de Leeuw, J. M. Mooij, T. Heskes, D. Posthuma, MAGMA: Generalized gene-set analysis of GWAS data. *PLOS Comput. Biol.* **11**, e1004219 (2015). doi: 10.1371/journal.pcbi.1004219; pmid: 25885710
90. S. Seabold, J. Perktold, paper presented at the 9th Python in Science Conference, Austin, TX, USA, 28 June to 3 July, 2010.
91. I. Tsatsani, DiPietroch, DaskalakisLab, DaskalakisLab/Daskalakis-Science2024: Daskalakis-Science2024v5, Zenodo (2024); https://zenodo.org/doi/10.5281/zenodo.10905726.

ACKNOWLEDGMENTS

We gratefully acknowledge the contributions in brain donation through the efforts of the staff at the Office of the Chief Medical Examiner of the State of Maryland, Western Michigan University Homer Stryker MD School of Medicine, the Department of Pathology, University of North Dakota School of Medicine and Health Sciences, the County of Santa Clara Medical Examiner-Coroner Office, and Gift of Life of Michigan. Appreciation is also expressed to the diagnostic team in the Genetic Neuropathology Section of the Lieber Institute for Brain Development. Lastly and most importantly, we extend our thanks to the families of our brain donors, who so generously agreed to participate in research. We acknowledge the members of two groups: (i) Traumatic Stress Brain Research Group: M. Friedman, N. Kowall, C. Brady, A. McKee, T. Stein, B. Huber, P. Holtzheimer, V. Alvarez, D. Benedek, R. Ursano, D. Williamson, D. Cruz, K. Young, J. Krystal, D. Mash, M. Hardegree, W. Scott, D. Davis, M. Girgenti, G. Serlin, B. Marx, T. Keane, M. Logue, E. Wolf, and M. Miller; and (ii) PsychENCODE Consortium: S. Abkarian, A. Abyzov, N. Ahituv, D. Arasappan, J. J. A. Armenteros, B. Beliveau, J. Bendl, S. Berretta, R. Bharadwaj, A. Bhattacharya, L. Bicks, K. Brennand, D. Capauto, F. Champagne, T. Chatterjee, C. Chatzinakos, Y. Chen, H.-C. Chen, Y. Cheng, L. Cheng, A. Chess, J.-F. Chien, Z. Chu, D. Clarke, A. Clement, L. Collado-Torres, G. Cooper, G. Crawford, R. Dai, N. Daskalakis, J. Davila-Velderrain, A. Deep, C. Deng, C. DiPietro, S. Dracheva, S. Drusinsky, Z. Duan Duan, D. Duong, C. Dursun, N. Eagles, J. Edelstien, P. Emani, J. Fullard, K. Galani, T. Galeev, M. Gandal, S. Gaynor, M. Gerstein, D. Geschwind, K. Girdhar, F. Goes, W. Greenleaf, J. Grundman, Q. Guo, C. Gupta, Y. Hadas, J. Hallmayer, X. Han, V. Haroutunian, N. Hawken, C. He, E. Henry, J. Heon Shin, S. Hicks, M. Ho, L.-L. Ho, G. Hoffman, Y. Huang, L. Huuki, A. H. Hwang, T. Hyde, A. Iatrou, F. Inoue, A. Jajoo, M. Jensen, L. Jiang, P. Jin, T. Jin, C. Jops, A. Jourdon, R. Kawaguchi, M. Kellis, J. Kleinman, S. Kleopoulos, A. Kozlenkov, A. Kriegstein, A. Kundaje, S. Kundu, C. L. Lee, D. Lee, J. Li, M. Li, X. Lin, S. Liu, J. Liu, J. Liu, C. Liu, S. Liu, S. Lou, J. Loupe, D. Lu, S. Ma, L. Ma, L. Ma, M. Margolis, J. Mariani, K. Martinowich, K. Maynard, S. Mazariegos, R. Meng, R. Meyers, C. Micallef, T. Mikhailova, G.-L. Ming, S. Mohammadi, E. Monte, K. Montgomery, J. Moore, J. Moran, E. Mukamel, A. Nairn, C. Nemeroff, P. Ni, S. Norton, T. Nowakowski, L. Omberg, S. Page, S. Park, A. Patowary, R. Pattni, G. Pertea, M. Peters, N. Phalke, D. Pinto, M. Pjanic, S. Pochareddy, K. Pollard, A. Pollen, H. Pratt, P. Przytycki, C. Purmann, Z. Qin, P.-P. Qu, D. Quintero, T. Raj, A. Rajagopalan, S. Reach, T. Reimonn, K. Ressler, D. Ross, P. Roussos, J. Rozowsky, M. Ruth, W. B. Ruzicka, S. Sanders, J. Schneider, S. Scuderi, R. Sebra, N. Sestan, N. Seyfried, Z. Shao, N. Shedd, A. Shieh, M. Skarica, C. Snijders, H. Song, M. State, J. Stein, M. Steyert, S. Subburaju, T. Sudhof, M. Synder, R. Tao, K. Therrien, L.-H. Tsai, A. Urban, F. Vaccarino, H. van Bakel, D. Vo, G. Voloudakis, B. Wamsley, T. Wang, S. Wang, D. Wang, Y. Wang, J. Warrell, Y. Wei, A. Weimer, D. Weinberger, C. Wen, Z. Weng, S. Whalen, K. White, A. Willsey, H. Won, W. Wong, H. Wu, F. Wu, S. Wuchty, D. Wylie, S. X. Xu, C. Yap, B. Zeng, P. Zhang, C. Zhang, B. Zhang, J. Zhang, Y. Zhang, X. Zhou, R. Ziffra, and T. Zintel.
Funding: This work was supported by NIMH (R01MH117291 to J.E.K., R01MH117292 and P50MH115874 to K.J.R., R01MH117293 to C.B.N., R01MH10659 to C.M.N. and K.J.R., and R21MH102834 to M.W.M.), the Brain & Behavior Research Foundation (2015 and 2018 NARSAD Young Investigator grants to N.P.D.), and Stichting Universitas/the Bontius Foundation (to N.P.D.). C.C. was supported by a Seed Grant (through NIMH P50-MH115874). C.S. was supported by the Dutch Research Council (NWO) fund (Rubicon) and McLean Hospital's Rappaport Award. C.P.D. was supported by an Administrative Diversity Supplement and a Seed Grant (through NIMH P50-MH115874). M.W.L was supported by a VA I01BX003477 grant. M.S.E.S. was supported by McLean Hospital's T32MH125786. **Author contributions:** Conceptualization: N.P.D., C.B.N., J.E.K., and K.J.R.; Project administration: N.P.D., C.B.N., J.E.K., and K.J.R.; Funding acquisition: N.P.D., C.B.N., J.E.K., and K.J.R.; Investigation: N.P.D., C.C., R.A.B., D.A., A.D.-S., D.M.D., R.T., J.T., F.A.C., T.H., N.T.S., J.H.S., D.R.W., C.B.N., J.E.K., and K.J.R.; Resources and data curation: N.P.D., C.S., L.C.-T., A.D.-S., M.W.L., A.X.M., M.W.M., C.M.N., and B.B.S.; Methodology: N.P.D., A.I., C.C., A.J., D.W., and L.C.-T.; Data preprocessing: N.P.D., A.I., C.C., A.J., C.P.D., I.T., D.A., L.C.-T., E.B.D., D.M.D., N.E., and G.P.; Formal analysis and software: N.P.D., A.I., C.C., A.J., D.W., C.P.D., I.T., and C.-Y.C. with contributions from C.S., C.D.P., M.S.-E., L.H., V.H., and M.S.E.S. and critical input from D.A., R.A.B., L.C.-T., S.W., D.R.W., C.B.N., J.E.K., and K.J.R.; Visualization: N.P.D., A.I., C.C., A.J., C.S., and D.W., with contributions from C.P.D., I.T., C.D.P., M.S.-E., L.C.-T., L.H., and J.F.L; Writing – original draft: N.P.D., A.I., A.J., C.S., and K.J.R. with contributions from D.W., C.P.D., C.D.P., M.S.-E., and J.F.L. and critical input from all authors; Writing – review and editing: N.P.D., A.I., A.J., C.S., and K.J.R. with contributions from D.W., I.T., C.D.P., and M.S.E. and critical input from all authors; Print summary – original draft: N.P.D. and A.I. with input from K.J.R.; Supervision: N.P.D., F.A.C., N.T.S., J.H.S., C.B.N., J.E.K., and K.J.R. **Competing interests:** Within the past 2 years, N.P.D. has been on scientific advisory boards for BioVie Inc., Circular Genomics, Inc., and Feel Therapeutics, Inc. For unrelated work, D.R.W. is on the advisory boards of Pasithea Therapeutics and Sage Therapeutics; D.D. is a cofounder of ARC Proteomics and cofounder and paid consultant of Emtherapro Inc.; C.-Y.C. is an employee of Biogen Inc.; M.S.E.S. receives consulting fees for unrelated work from Niji Corp; B.B.S. is an employee and stockholder of Biogen Inc.; and K.J.R. has received consulting income from Alkermes and sponsored research support from Brainsway and Takeda and is on the scientific advisory boards for Janssen, Verily, and Resilience Therapeutics. All other authors declare no competing interests. **Data and materials availability:** The source data described in this manuscript are available through the PsychENCODE Knowledge Portal (https://www.psychencode.org/). The PsychENCODE Knowledge Portal is a platform for accessing data, analyses, and tools generated through grants funded by the National Institute of Mental Health (NIMH) PsychENCODE Consortium. Data are available for general research use according to the consortium requirements for data access and data attribution. For access to content described in this manuscript, see https://doi.org/10.7303/syn25611941 and

https://doi.org/10.7303/syn51217925. All analysis code and scripts are available on GitHub at https://github.com/DaskalakisLab/Daskalakis-Science2024 and Zenodo (*91*). The GWAS summary statistics are available by the Psychiatric Genomics Consortium (PGC) at https://pgc.unc.edu/for-researchers/download-results/. The MVP GWAS summary statistics are made available through dbGAP request study_id=phs001672.v11.p1 (https://www.ncbi.nlm.nih.gov/projects/gap/cgi-bin/study.cgi?study_id=phs001672.v11.p1).

SUPPLEMENTARY MATERIALS

science.org/doi/10.1126/science.adh3707
PTSD Working Group of Psychiatric Genomics Consortium Collaborators
Materials and Methods
Supplementary Text
Figs. S1 to S19
Captions for Tables S1 to S13
References (*92*–*151*)
Tables S1 to S13

Submitted 22 March 2023; resubmitted 18 January 2024
Accepted 5 April 2024
10.1126/science.adh3707